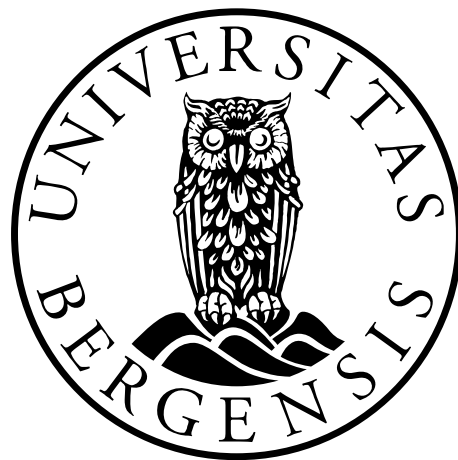


# **Study of the seismic source parameters and its relation with other seismic engineering parameters**

**Quetzalcoatl Rodríguez Pérez**



Dissertation for the degree philosophiae doctor (PhD)  
at the University of Bergen

February 2013



## **Preface**

The study presented in this thesis was initiated in January 2010 when I was enrolled in the Ph.D program at the University of Bergen (UiB). The research was mainly funded by the Mexican National Council for Science and Technology (CONACYT), and partially by the Department of Earth Science at UiB. The thesis work was completely conducted at the University of Bergen. This thesis consists of two parts. The first part focuses on the general theoretical background and methodology used in this study and describes the main scientific contributions that make up the main body of the thesis. The second part presents a collection of four research publications, which is the main outcome of my work. Out of these four publications, the first one is published, the second one is accepted for publication, and other two papers have been submitted to peer-review journals. The thesis provides information about seismic source parameter estimates, source scaling, and ground motion simulation using different techniques and data. I have worked with two different tectonic settings, the transform plate fault systems in Baja California area, and the Mexican subduction zone, but most of my work is based on the latter zone. The study also highlights the differences in source parameters and ground motions among near-trench, interplate, and normal inslab subduction earthquakes. Special focus has been given in developing finite-fault scaling relations and ground-motion attenuation relationships to provide useful models for future seismological studies.

Quetzalcoatl Rodríguez Pérez

February 2013

## Acknowledgements

I am grateful to the Mexican National Council for Science and Technology (CONACYT) for financing my studies. Additional funding for conferences was kindly provided by the Geodynamics Group of the Earth Science Department at the University of Bergen (UiB). I would like to thank all the institutions that provided data for this study, specially to the Servicio Sismológico Nacional (SSN), and the Red Sísmica del Noreste de México (RESNOM) operated by Instituto de Geofísica of the Universidad Nacional Autónoma de México (UNAM), and by the Centro de Investigación Científica y de Educación Superior de Ensenada (CICESE), respectively.

I express my deep gratitude to my main supervisor Professor Lars Ottemöller for guidance and support during my Ph.D studies. I am also very grateful to my co-supervisors Professors Kuvvet Atakan and Mathilde B. Sørensen for their academic support during my Ph.D studies. I would like to thank Professor Emeritus Jens Havskov, Dr. Mohammad Raeesi, and Dr. Louise Wedderkopp Bjerrum for their help. I thank Dr. Carlos M. Valdés González chief of the SSN for kindly providing access to the seismic data. I would like to thank the staff in the Earth Science Department for their help during my stay. Among them I would like to mention Kristin Miskov Nodland, Hanne Israelsen, Caroline Ertsås Christie, Trine Lise Stjernholm and Berit Marie Storheim.

*To my family,*

*"Seek the truth  
hear the truth  
learn the truth  
love the truth  
speak the truth  
hold the truth  
and defend the truth until death."*

*Jan Hus 1369-1415*



## Abstract

The term seismic source refers to the sources which can generate seismic waves. The seismic source of tectonic earthquakes is represented as a displacement discontinuity on a plane surface as a result of shear faulting. Earthquakes can be defined as a rapid release of strain energy caused by tectonic forces. The elastic wave radiation carries with it information concerning the parameters of faulting or seismic source parameters, so estimating them provides us valuable information about the rupture process. For example, the seismic moment is a measurement of the earthquake size, the radiated energy is a fundamental parameter of the strength of seismic waves generated by an earthquake, and the stress drop provides information about earthquake mechanics. In the present study, two applications of source parameters are conducted. First, the use of earthquake source parameters for estimating scaling laws needed for seismic hazard purposes. Second, the use of seismic source parameters in ground motion simulations. The thesis focuses on two different tectonic regions: the transform fault systems in the Baja California area, and the Mexican subduction zone. In each tectonic area, the earthquakes have different characteristics such as how faults rupture, how waves propagate, attenuate, or disperse through the Earth. In paper 1, a source study and stochastic finite-fault ground simulation is carried out for the 4 April 2010  $M_w = 7.2$  El Mayor-Cucapah earthquake, a crustal strike-slip event in Baja California. This region is seismically active with strike-slip earthquakes ( $M \sim 7$ ), but most of them were poorly recorded in the past. The El Mayor-Cucapah earthquake is a well-instrumented event, allowing the study of the source complexities and site effects at soil and rock site conditions. High amplification was observed on soil stations. Teleseismic waveform inversion shows that the slip distribution consisted of two asperities. Source time function analysis and near-fault ground-motion records show also that the mainshock consists of at least two subevents. This event also illustrates important differences with respect to the subduction zone events, such as long rupture length ( $\sim 140$  km), high stress drop, and long source time function.

In paper 2, a comparative source parameter analysis between continental and oceanic strike-slip events, and subduction thrust events is carried out. The results support the observation of mechanism dependence of radiated energy and apparent stress reported in previous studies. Most of the scaling relationships commonly used are based on crustal events, and recently some relations for subduction zone based on global datasets have been developed, but those relations not necessary describe the source parameters for the Mexican subduction zone. In paper 2, finite-fault scaling relationships for interplate thrust subduction earthquakes are developed by examining the slip distribution of 15 earthquakes ( $6.5 < M_w < 8.0$ ) imaged from teleseismic data with an iterative deconvolution method. The obtained models can be used in seismic hazard assessment in Mexico. Asperities have a significant role in the rupture process due to larger slip and stress drop than for the background area. Previous studies show that the asperity areas, as well as entire rupture areas, scale with seismic moment and some relations for source parameters have been developed. Within paper 2, heterogeneous slip models (5 strike-slip;  $6.5 < M_w < 7.2$ , and 15 thrust events) were characterized by determining source parameters on the asperities and on the background area. The results show that the area of the asperities represented about 22 % and 24 % of the total area for strike-slip, and thrust events, respectively. In paper 3, different types of subduction zone earthquakes in the Guerrero seismic gap zone (interplate  $M_w = 6.6$ , thrust near-trench  $M_w = 6.7$ , and normal inslab  $M_w = 6.5$ ) are analyzed in terms of source parameters and ground-motion observations. The similarity in magnitude, gives the opportunity to compare the results for the three different types of earthquake and interpret them in terms of the tectonic environments, and seismic hazard. Different methods are used to estimate source parameters in order to observe mainly differences in stress-drop, and radiated energy. The results support the observation that the near trench event has the lowest source parameters ( $\Delta\sigma$ ,  $E_R$ , and  $E_R/M_o$ ) while the highest values correspond to the normal inslab earthquake. By comparing the radiation efficiency ( $\eta_{inslab} < \eta_{interplate} < \eta_{near-trench}$ ), it is observed that the inslab event has the most efficient rupture mechanics. Source parameter estimates were validated through



the stochastic simulations showing that the peak ground acceleration observations can be explained by a stress-drop of 0.38, 3.40, and 34.20 MPa for the near-trench, near-coast, and inslab events, respectively. Ground-motion attenuation relationships are an important tool in seismic risk assessment. In Mexico, most of the effort in this issue has been addressed to develop ground motion models for interplate and inslab earthquakes in central Mexico. No ground-motion attenuation relationships for near-trench events in the Mexican subduction zone and normal inslab events in southern Mexico have been developed. In paper 4, regression models to predict pseudoacceleration response spectra (5% damping), peak ground acceleration, and peak ground velocity for thrust, near-trench events were developed using the one-stage maximum likelihood method. Comparison of the inslab PGA curve of this study and the reported one for central Mexico, suggests that events in southern southern Mexico decay somewhat faster than events in the central region. The results obtained in the thesis can help in better understanding the seismic source and seismic hazard in Mexico.



## List of publications

1. Rodríguez-Pérez, Q., Ottemöller, L., and Castro-Escamilla, R. R. (2012). Stochastic finite-fault ground-motion simulation and source characterization of the 4 April 2010  $M_w$  7.2 El Mayor-Cucapah earthquake, *Seismological Research Letters*, 83, 235-249.
2. Rodríguez-Pérez, Q., and Ottemöller, L.(accepted). Finite-fault scaling relations in Mexico, submitted to *Geophysical Journal International*.
3. Rodríguez-Pérez, Q., Ottemöller, L., and Raeesi, M (submitted). Source study of three moderate size recent earthquakes in the Guerrero seismic gap and its tectonic implications, submitted to *Bulletin of the Seismological Society of America*.
4. Rodríguez-Pérez, Q. (submitted). Ground-motion attenuation relationships for near-trench and normal-faulting subduction zone earthquakes in Mexico, submitted to *Bulletin of the Seismological Society of America*.



# Contents

<b>PREFACE.....</b>	<b>I</b>
<b>ACKNOWLEDGEMENTS.....</b>	<b>II</b>
<b>ABSTRACT.....</b>	<b>V</b>
<b>LIST OF PUBLICATIONS.....</b>	<b>IX</b>
<b>CONTENTS.....</b>	<b>XI</b>
<b>PART I. SUMMARY.....</b>	<b>1</b>
<b>1.INTRODUCTION.....</b>	<b>3</b>
<b>2. TECTONIC SETTING AND SEISMICITY OF MEXICO.....</b>	<b>5</b>
2.1 SEISMOTECTONICS OF BAJA CALIFORNIA.....	5
2.2 SEISMOTECTONICS OF THE MEXICAN SUBDUCTION ZONE.....	7
2.3 THE GUERRERO SEISMIC GAP.....	9
2.4 INSLAB SEISMICITY IN CENTRAL AND SOUTHERN MEXICO.....	10
<b>3. THEORY AND METHODS.....</b>	<b>12</b>
3.1 FOCAL MECHANISM AND SEISMIC MOMENT.....	16
3.2 SOURCE TIME FUNCTION, DURATION, AND DIRECTIVITY.....	17
3.3 STRESS DROP.....	18
3.4 RADIATED SEISMIC ENERGY.....	20
3.5 APPARENT STRESS, $E_R/M_o$ RATIO, SEISMIC EFFICIENCY .....	22
3.6 SEISMIC SCALING RELATIONSHIPS.....	25
3.7 ITERATIVE DECONVOLUTION MOMENT TENSOR INVERSION.....	27
3.8 GROUND-MOTION PARAMETERS.....	31
3.9 GROUND-MOTION ATTENUATION RELATIONSHIPS.....	32
3.10 THE STOCHASTIC METHOD.....	35
<b>4. RESULTS.....</b>	<b>38</b>
4.1 STOCHASTIC FINITE-FAULT GROUND-MOTION SIMULATION AND SOURCE CHARACTERIZATION OF THE 4 APRIL 2010 $M_w$ 7.2 EL MAYOR-CUCAPAH EARTHQUAKE (PAPER 1).....	38
4.2 FINITE-FAULT SCALING RELATION IN MEXICO (PAPER 2).....	39
4.3 SOURCE STUDY OF THREE MODERATE SIZE RECENT EARTHQUAKES IN THE GUERRERO SEISMIC GAP AND ITS TECTONIC IMPLICATIONS (PAPER 3).....	40

4.4 GROUND-MOTION ATTENUATION RELATIONSHIPS FOR NEAR-TRENCH AND NORMAL-FAULTING INSLAB SUBDUCTION ZONE EARTHQUAKES IN MEXICO (PAPER 4).....	42
<b>5.CONCLUSIONS AND FUTURE PERSPECTIVES.....</b>	<b>44</b>
5.1 FUTURE PERSPECTIVES.....	45
<b>REFERENCES.....</b>	<b>48</b>
<b>PART II. PUBLICATIONS.....</b>	<b>57</b>
PAPER I.....	59
PAPER II.....	77
PAPER III.....	121
PAPER IV.....	161

## **Part I. Summary**





# 1. Introduction

Earthquakes are one of the most devastating natural hazards producing damage that can result in human fatalities. Seismologists focus on understanding and analyzing their behavior to prevent destruction and loss of life. Seismograms are represented as the convolution of the source, the path of the seismic waves, and the site where it is recorded. The study of the seismic source is of great importance in seismology, allowing us to understand the physics of the earthquakes. Seismic source parameters are used to quantify earthquakes in order to obtain parameters such as the size of the event, the fault geometry, the rupture process, type of faulting, source directivity or radiation pattern. Estimating the size of an earthquake is very important in seismic hazard assessment. The size of earthquakes is measured from the amplitude of the seismic waves and is given in terms of the seismic moment ( $M_o$ ) (or moment magnitude  $M_w$ ). Moment magnitude is a key input parameter for source scaling relationships and for engineering ground motion models or ground-motion attenuation relationships. Scaling relationships are models among the different source parameters, and they could be obtained theoretically or empirically. Empirical scaling relationships are derived from source parameters compiled for many earthquakes. The main application of the source scaling relationships is to estimate source parameters for an earthquake. A ground-motion attenuation relationship is a model that relates a specific strong-ground motion parameter to seismological parameters of an earthquake. There are two types of ground motion parameters: 1) peak time-domain parameters; and 2) peak frequency-domain parameters. For engineering purposes, peak time-domain parameters such as peak ground acceleration (PGA), peak ground velocity (PGV), and peak ground displacement (PGD) have been used to represent short, mid, and long period components of the ground motion. Response spectrum is used in seismic design procedures where the natural period of a structure is incorporated. The most common peak frequency-domain parameter is the pseudo acceleration (PSA). Ground-motion attenuation relationships characterize the earthquake

source, the wave propagation path, and soil conditions. These types of models are used to evaluate seismic hazard at specific sites. Stress-drop accounts for the amount of stress that is released during an earthquake. Stress drop is an important parameter in the estimation of strong ground motions because it controls the level of peak ground acceleration. Kinematic source models are used to study the earthquakes rupture. In these models, the wave-field is calculated for a predetermined fault using the elastic theory. The slip distribution on the fault is determined by the inversion of the observed seismic data. Kinematic models show the complexity of earthquake source and the resulted slip distributions are heterogeneous in space. Areas on the fault plane which show large slip relative to the average slip over the entire fault plane are called asperities. These regions are responsible for a large part of the stress release. Source parameters on the asperities and background areas can be used to develop empirical scaling relations useful to improve ground motion predictions. These points constitute the core of the research.

## 2. Tectonic setting and seismicity of Mexico

Seismic source parameters are controlled by the tectonic environment. The tectonic stress field determines the type of faulting and the elastic rock properties control the earthquake occurrence, attenuation and propagation of the seismic waves. Another example is the seismogenic zone which varies with the tectonic environment, so differences in source scaling are expected. In this section, the basic tectonic framework for Mexico is explained. Mexico is one of the most seismically active areas in the world. The country is located atop four major tectonic plates and one microplate: the North American (NA), the Cocos (CO), the Caribbean (CA), the Pacific (PA); and the Rivera (RI) plates, respectively (Figure 1). Mexico can be divided into two main tectonic regions corresponding to the Gulf of California and to the Mexican subduction zone. These regions differ in many characteristics such as the tectonic stress regime, convergence rate between the plates, seismogenic zone and seismicity.

### 2.1 Seismotectonics of Baja California

The plate boundary between the PA and NA plates is a transform fault type boundary with small spreading centers (Figure 2). The spreading segments are connected by long transform faults. The region is dominated by a strike-slip fault stress regime. The relative motion of the PA plate with respect to the NA plate is 4.8 cm/yr (DeMets *et al.*, 1995). The majority of the seismicity is caused by the right lateral transform faults, where the largest events can reach magnitudes of  $6.0 < M_w < 7.5$ . In the pull-apart basins, the seismic activity is generally characterized by lower magnitude earthquakes and corresponds mainly to normal fault mechanisms (Goff *et al.*, 1987). The continental segment of Baja California is affected by a number of regional-scale active faults that are part of a complex lateral system (Goff *et al.*, 1987). One of these regional faults is the Laguna Salada fault system where the 4 April 2010  $M_w = 7.2$  El Mayor-Cucapah

earthquake occurred. For purposes of the thesis, the description will focus only on this fault system. The Laguna Salada fault system is composed of two faults, a relatively simple fault in the north, the Laguna Salada fault, and a more complex system in the south and east. The latter is a family of faults, one of them is the Cucapah fault. The fault length could generate events with magnitudes ranging from 6.5 to 7.5 (Jennings, 1994). The earthquake recurrence interval is unknown because of the lack of information about the seismicity in the area. The El Mayor-Cucapah earthquake is the largest earthquake in the area since the Laguna Salada earthquake in 1892 ( $M = 7-7.5$ ).

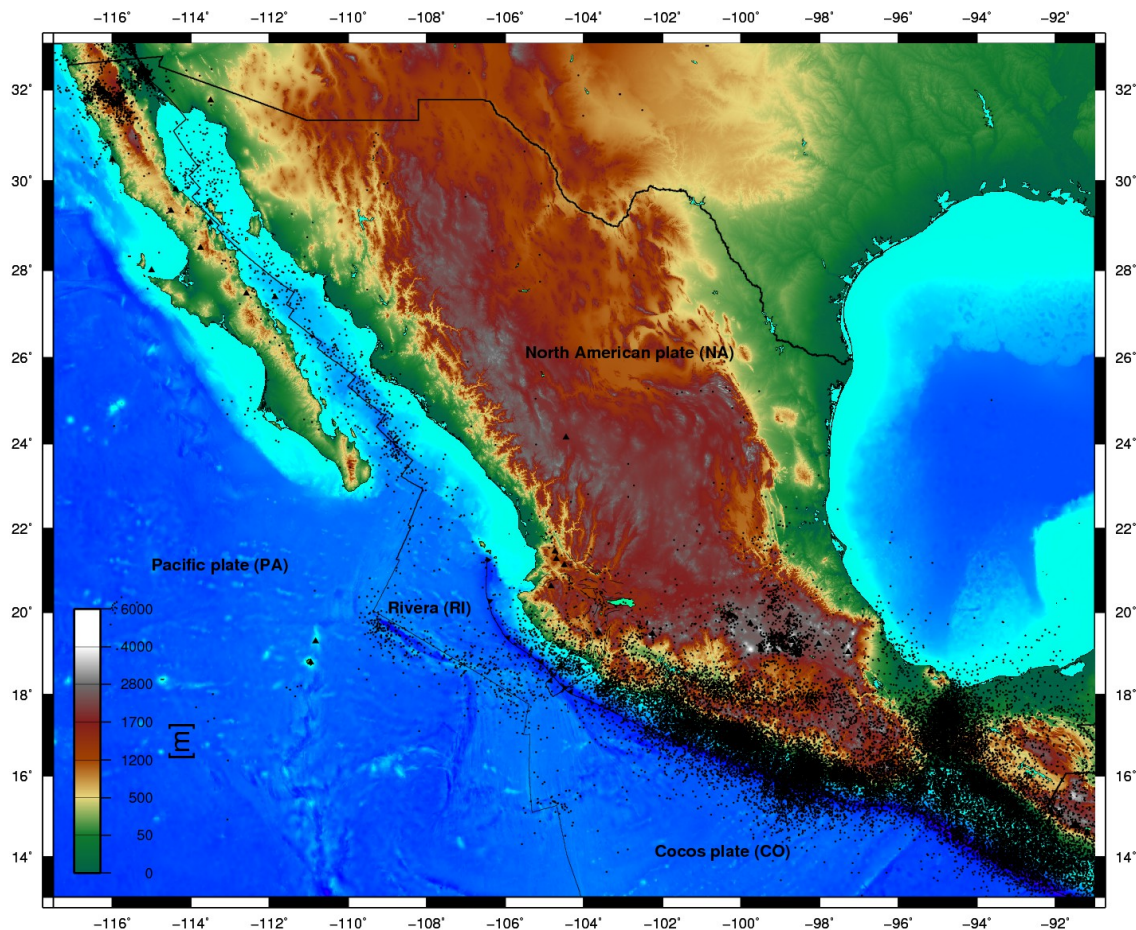


**Figure 1.** Tectonic map of Mexico and seismicity in the period of 1978-2008 reported by the Mexican National Seismological Service (SSN). Black triangles are volcanoes.

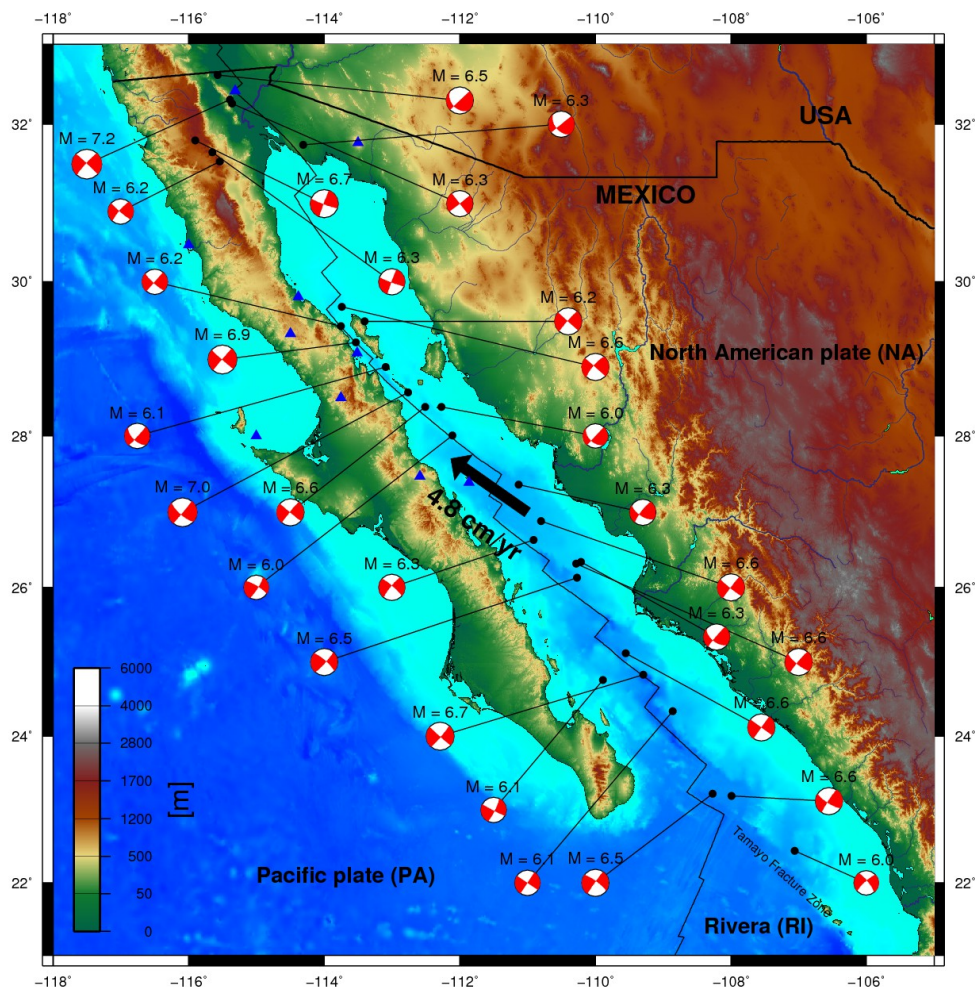


**Figure 2.** Major strike-slip earthquakes ( $6.0 < M_w < 7.2$ ) in the Baja California region in the period of 1956-2012. The relative motion of the PA plate with respect to the NA is 4.8 cm/yr. Blue triangles are volcanoes. Focal mechanisms taken from Harvard global CMT catalog.

## 2.2 Seismotectonics of the Mexican subduction zone

The Mexican Pacific margin has mainly developed by subduction of the NO, CO, and RI plates along the Middle America trench (MAT). The MAT extends from the Gulf of California at the intersection with the Tamayo fracture zone to Costa Rica. The Mexican subduction zone has experienced several thrust earthquakes of great magnitude ( $7.0 < M_w < 8.2$ ) over the last century (Figure 3). Paleoseismology studies show that the subduction zone is able to generate

tsunami events as large as the 28 March 1787 event ( $M = 8.6$ ) (Suárez and Albini, 2009). The rupture areas of the last earthquakes show a seismic gap in the Mexican subduction zone (Figure 3), the Guerrero seismic gap (GG) with a length of about 200 km. If the entire gap were to rupture in an earthquake, the size of the event could reach a magnitude of 8.1–8.4 (Singh and Mortera, 1991). In the Tehuantepec zone (TZ), no significant thrust earthquake has occurred over the last 180 years, and it is considered to be either aseismic or seismic with anomalously long recurrence intervals for major earthquakes which might be due to the subduction of the Tehuantepec ridge (Astiz and Kanamori, 1984). The Rivera plate has a convergence rate of 2.5 cm/yr relative to North America (Figure 3) (DeMets *et al.*, 1994). The convergence rate of the CO plate relative to NA plate ranges from 5.2 cm/yr to 7.05 cm/yr in the Jalisco-Michoacan area and Chiapas, respectively (Figure 3) (DeMets *et al.*, 1994).

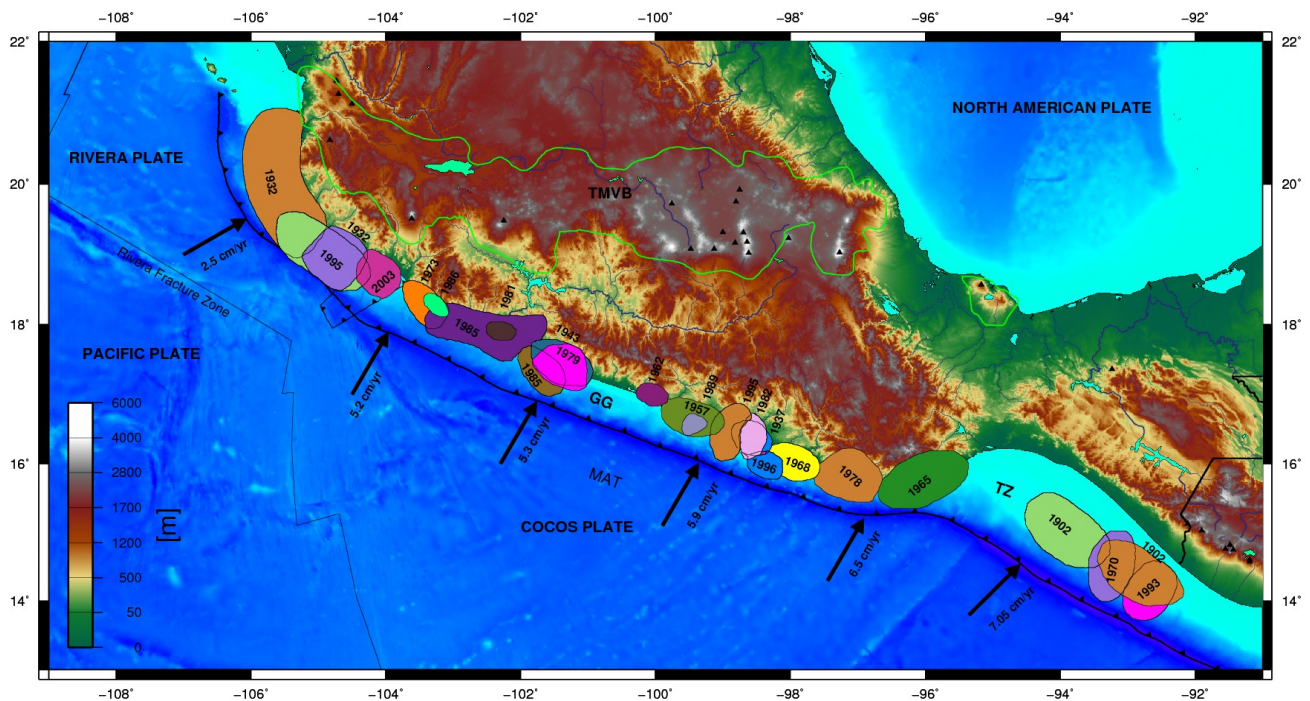


**Figure 3.** Large thrust interplate earthquakes of this century. Color areas show rupture areas for these events. GG is the Guerrero seismic gap, TMVB is the Trans-Mexican volcanic belt, TZ is the Tehuantepec ridge zone, and MAT is the Middle American trench (modified from Kostoglodov and Pacheco, 1999).

The geometry of the subducted slab varies from north to south. The slab initially dips at an angle of  $9^\circ$  to  $16^\circ$  down to mantle depths of 20 km, gradually increasing to about  $50^\circ$  at depths below 40 km (profile A in Figure 4) (Pardo and Suarez, 1993). The subduction in Michoacan coast represents a transition zone from a steep subduction angle of the Rivera plate to almost subhorizontal angle in central Mexico (profile B in Figure 4) (Pardo and Suarez, 1995). In the southern part, the dip angle of the subducted slab increases from  $25^\circ$  just NW of the Tehuantepec ridge in Oaxaca to  $\sim 40^\circ$  southeast of the Tehuantepec ridge in Chiapas state (profile E in Figure 4) (Rebollar *et al.*, 1999; Bravo *et al.*, 2004).

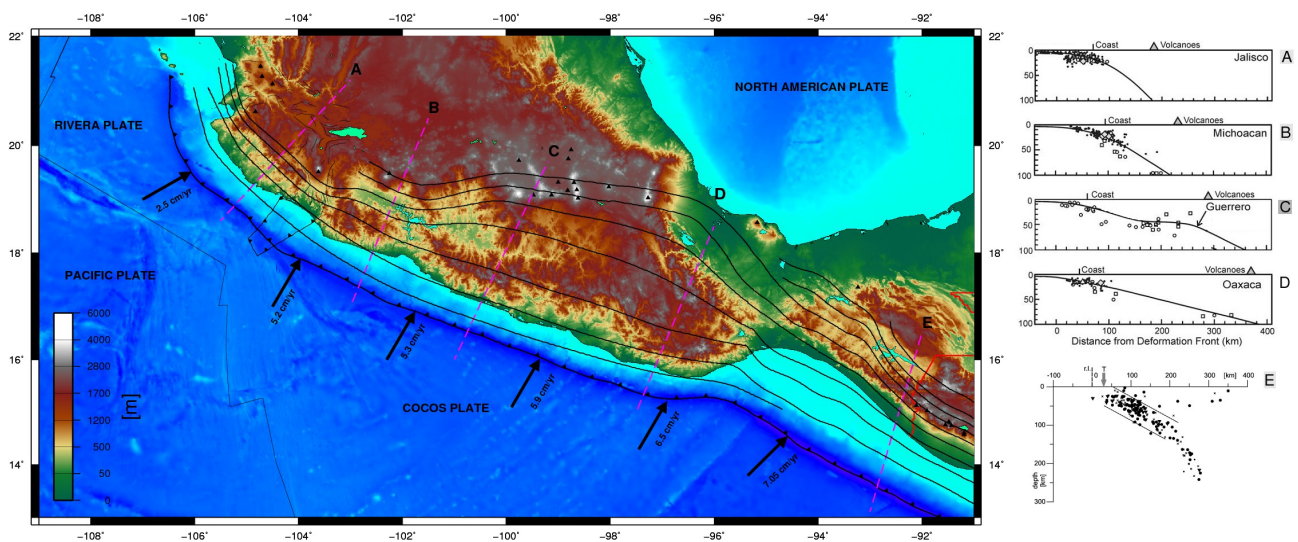


**Figure 4.** Tectonic map showing the location of the subduction cross sections: A, Jalisco; B, Michoacan; C, Guerrero; D, Oaxaca; and E, Chiapas. Arrows show the converge rate of the Cocos and Rivera plate with respect to North American plate. Right column shows the Wadati-Benioff zone for selected cross sections (cross sections from Currie *et al.*, 2001; and Špičák *et al.*, 2007).

### 2.3 The Guerrero seismic gap

This zone has experienced several thrust earthquakes of large magnitude ( $M_w > 7.0$ ), but is considered a seismic gap as it has not seen a large event since 1911

( $M_w = 7.5$ ). Considering the convergence rate of the CO plate and the recurrence time of the last earthquake in the GG, 5.5 m of elastic displacement have been accumulated. In the NW part of the GG, the last significant thrust earthquakes are: the 1943 Guerrero earthquake ( $M_w = 7.4$ ), the 1979 Petatlan earthquake ( $M_s = 7.6$ ) and the 1985 Zihuatanejo earthquake ( $M_s = 7.5$ ). Significant thrust earthquakes on the SE part of the GG also happened in 1957 ( $M_w = 7.8$ , Costa Chica) and in 1962 ( $M_w = 7.0, 7.1$ , Acapulco). The accumulated strain has generated only a few  $M_w \sim 6 - 6.5$  events near the edges of the GG, for example the 1996 ( $M_w = 6.6$ ), 2002 ( $M_w = 6.7$ ) and 2010 Guerrero earthquakes ( $M_w = 6.5$ ) studied in paper 3. The updip and downdip limits of the seismogenic zone are critical for estimation of tsunami and seismic hazard. These limits define the maximum earthquake rupture width expected during a great shallow thrust earthquake based on the updip limit, thought to be at 5 km and the downdip limit has been estimated in the range of 80 – 120 km (Pacheco and Singh, 2010). Slow slip events (SSEs) have been observed at the Mexican subduction zone. SSEs are located at the downdip extension of the seismogenic zone. In the Guerrero, the reported SSEs have a periodicity of about 4 years with equivalent magnitudes of  $M_w \sim 7.5$  (e.g. Lowry *et al.*, 2001; Kostoglodov *et al.* 2003; Larson *et al.*, 2007; Vergnolle *et al.*, 2010). The relation between SSEs and earthquakes in the GG is not clear, but it is thought that SSEs are an important part of the strain release process and the seismic cycle, because they could modify the loading and releasing on the plate interface and can affect the recurrence of large thrust earthquakes.

## 2.4 Inslab seismicity in Central and Southern Mexico

Shallow normal inslab earthquakes have caused significant damage to cities in the Mexican altiplano (e.g. 1999 Tehuacan earthquake,  $M_w = 6.9$ ). In general, shallow inslab earthquakes at subduction zones occur downdip from the coupled interface. In the central segment of the Mexican subduction zone some inslab events occur



immediately below or near the edge of the coupled interface which is not common for other inslab events (Singh *et al.*, 2000). Inslab events have an important role in the seismic cycle. They usually occur before large thrust interplate events, the intraplate events are tensional in the downdip subducted slab and compressional in the outer rise, or after large thrust interplate events the downdip events become either compressional or less frequently tensional, and the events in the outer rise become tensional (Lay *et al.*, 1989). In Mexico, some of the large downdip tensional events follow the thrust earthquakes rather than precede them (Singh *et al.*, 2000). In southern Mexico, normal intermediate-depth earthquakes can reach depths of about 200 km. These events are associated mainly to down-dip tension of the slab.

### **3. Theory and methods**

The term seismic source is used to describe the source or the origin of the seismic waves. There are two main categories of seismic sources: natural sources and man-made sources. Tectonic earthquakes are an example of natural seismic sources and they are caused when the brittle part of the Earth's crust is subjected to stress that exceeds its breaking strength. Earthquake is the term used to describe both sudden slip on a fault, and the resulting ground shaking and radiated seismic energy.

The parameters that describe the rupture process are called seismic source parameters. Seismic source characterization is an important part in ground motion prediction, earthquake physics and seismic hazard assessment. In ground motion prediction, source parameters are used to simulate ground motions generated by earthquakes. The important parameters that control the ground motion level are the stress drop and the seismic moment. In earthquake physics, source parameters are used to quantify the physical properties of the earthquakes such as the earthquake size, the radiated energy, the dimensions of the fault, the rupture velocity, the type of faulting, etc. These physical properties vary with the type of faulting making necessary to analyze the differences among them. In seismic hazard assessment, source parameters are used to develop two kind of models or relationships: 1) scaling relationships and 2) ground-motion attenuation relationships. Scaling relationships are relations among seismological parameters. Most of the scaling relationships relate moment magnitude or seismic moment with other parameter because seismic moment quantifies the earthquake size. Ground-motion attenuation relationships are relations among the seismic source parameters and ground motions. The objective of both relationships is to estimate unknown ground motions or source parameters for given input parameters.

Recently, source studies focused on characterizing source properties on heterogeneous slip models (Somerville *et al.*, 1999). Source parameters derived from slip distributions provide an insight into the rupture process. Slip distribution source analysis is based on the contrast in seismic source parameters on regions on the fault plane that have larger slip compared to the average slip known as asperities and the background area. Estimations of size, slip and stress drop of the asperities are important for source modeling and more accurate ground motion prediction. Estimation of source parameters and asperity characterization from finite-fault models is one of the main issues of this thesis.

The study of the seismic source is not a simple task. Therefore, a collection of techniques are used to have a comprehensive understanding of the seismic source. The methodology used in this work consists mainly of four parts: 1) source parameter estimation; 2) establishment of relations among parameters (source scaling relationships); 3) validation of the source parameters through ground motion simulations; and 4) establishment of relations between seismological source parameters and ground motion parameters (ground-motion attenuation relationships).

#### *Source parameter estimation*

Source parameters are estimated using different methods and data. Some of the techniques used in the thesis are teleseismic body-wave inversion, spectral analysis, and theoretical models. A more detailed description of these techniques is given in the following sections. The studied parameters are: fault dimensions, average displacement, maximum displacement, stress drop, radiated seismic energy, apparent stress, radiation efficiency, radiated energy to seismic moment ratio.

Fault dimensions are initially estimated from aftershock distributions. These dimensions are given as input to the slip inversion. The actual fault size is often less than the fault model size used in the inversion because the obtained slip patterns can result in regions on the fault that have almost zero slip. Therefore, the effective source dimensions defined by Mai and Beroza (2000) are adopted to accurately describe fault dimensions. The next parameter to be estimated is the stress drop. The concept of stress drop is explained in section 3.3. The static stress drop is calculated based on theoretical formulations using the fault dimensions (Kanamori and Anderson, 1975).

Some parameters are determined with the teleseismic body-wave inversion through forward modeling in a trial and error process such as the rupture velocity. Teleseismic inversion is explained in section 3.7. The parameters resulted from inversion are: focal mechanism, seismic moment, moment magnitude, duration, maximum displacement, and spatial distribution of slip on the fault plane.

Radiated seismic energy can be estimated from teleseismic (Boatwright and Choy, 1986) and regional (Singh and Ordaz, 1994) records. The radiated energy to seismic moment ratio is estimated using teleseismic data because estimation of the seismic moment from long-period waves is more reliable. The radiation efficiency is estimated using the static stress drop and teleseismic radiated seismic energy.

Source parameters on the asperities are obtained from the slip distributions. The first step is to define the asperities. Two definitions of asperities are used: based on maximum displacement (Mai and Beroza, 2005) and average slip (Somerville *et al.*, 1999). The second step is to quantify the source parameters. The parameters analyzed are: stress drop on the asperities, number of asperities, combined area of asperities, and the combined area of asperities to effective rupture area ratio.

### *Source scaling relationships*

After estimating seismic source parameters, the empirical source scaling relationships are obtained by regressions analysis. Previous studies have shown that many source parameters scale linearly with seismic moment (Kanamori and Anderson, 1975). Source parameters in the asperity regions also follow this linear behavior (Somerville *et al.*, 1999). The orthogonal regression is adopted to develop the regression analysis because it minimizes the Euclidean distance to the regression line, instead of the vertical distance, and is therefore, a better choice than the least squares regression (Blaser *et al.*, 2010). The obtained relations are compared with other subduction zones studies (e.g. Blaser *et al.*, 2010; Strasser *et al.*, 2010). Section 3.6 provides more information about source scaling.

### *Validation of the source parameters through ground motion simulations*

Ground motion prediction requires the study of the seismic source. One strategy to validate the estimated seismic source parameters is through forward modeling. The finite-fault stochastic method (Boore, 1983; Beresnev and Atkinson, 1997; Motazedian and Atkinson, 2005) is adopted to model ground motions because this method is easy to implement, widely used and incorporates fault geometry. In this method, the source parameters are used to generate the source spectra for a given earthquake. The stochastic method simulates the Fourier amplitude spectra as a result of contributions from the seismic source, path and site. The method is used to simulate strike-slip, normal, and thrust events and shows to be efficient in ground motion prediction. The stochastic method is explained in section 3.10.

### *Ground-motion attenuation relationships*

Another important application of the seismic source parameters is the development of ground-motion attenuation relationships. They are used to

estimate ground-motion values for an earthquake given the magnitude, distance, soil conditions, hypocenter depth, etc. The ground motion parameters analyzed are the peak ground acceleration, peak ground velocity and the response spectra. The relations are obtained by multivariate regression analysis. Traditionally, the relations are constructed by fitting the data to certain functional forms, using the least-squares method. Previous studies show that the decay of ground motions with distance could not correctly be estimated with this method because it neglected the correlation between the observations recorded at different sites for a given earthquake (Joyner and Boore, 1993). The one-stage maximum likelihood method solves this problem (Joyner and Boore, 1993). Another reason to select this method is that normal inslab ground-motion attenuation relationships for central Mexico were derived using this method. The method is also used in global studies (Atkinson and Boore, 2003). It allows the comparison of the obtained relationships for normal inslab earthquakes in southern Mexico and previous studies. The one-stage maximum likelihood method is explained in section 3.9.

The following sections provide a description of seismological concepts and methods used in this study.

### 3.1 Focal mechanism and seismic moment

One of the first parameters to be determined is the type of faulting or focal mechanism. Three basic types of faulting exist, normal faulting, reverse or thrust faulting and strike-slip or lateral faulting. The description of a fault is given by the strike, slip and rake angles which together define a focal mechanism. Focal mechanisms are important because the pattern of seismic waves depends on the fault geometry. For example, thrust faulting causes higher ground motion than strike-slip or normal faulting (Campbell, 1981). Focal mechanisms are also important for seismotectonic understanding of the region.

---

The size of the earthquake is another important parameter. Seismic moment ( $M_o$ ) is an accurate physical quantification of the size. Seismic moment is defined as  $M_o = \mu DS$ , where  $\mu$  is the rigidity,  $D$  is the average displacement, and  $S$  is the rupture area. Most of the magnitude scales are defined by wave amplitudes with corrections for attenuation, but these magnitudes cannot be related to any physical parameter of the source. Moment magnitude ( $M_w$ ) gives a magnitude directly related to the source process and does not saturate. Seismic moment can be estimated with geological or seismic methods. Estimate  $M_o$  or  $M_w$  is also important because it is an input parameter for many source scaling and ground-motion relations. In this study, focal mechanism solutions and seismic moment are estimated with the iterative deconvolution method (Kikuchi and Kanamori, 1991) using teleseismic data. The method is described in section 3.7.

### 3.2 Source time function, duration, and directivity

An important part for describing the seismic source process is the source time function. Source time function represents the slip history with time. Source time functions have irregular forms reflecting the source complexities. The source finiteness and the rupture propagation have an important effect on seismic radiation. This effect, called directivity, is similar to the Doppler effect. Directivity has an important influence on ground motions. At sites towards the rupture propagation, more energy arrives in shorter time, while in the opposite direction less energy arrives over a longer time. The duration of the radiated pulses is proportional to the length divided by the rupture velocity ( $\tau = L/V_r$ ). Rupture velocity is difficult to estimate from seismic data. In this study, rupture velocity is estimated through forward modeling as input parameter for teleseismic inversion. In general, for most of the large shallow earthquakes,  $V_r$  is approximately 75-95% of the  $S$ -wave velocity.

In practice, the extraction of the source time function requires separation of the propagation, site, and instrumental response effects from recorded seismograms. These can be solved with the empirical Green function technique (Hartzell, 1978; Mueller, 1985). The technique involves the deconvolution of the mainshock and a small event (an empirical Green function, EGF) at the same stations. EGF constitutes an approximate point-source impulse response for a given moment tensor. For simplicity the deconvolution is done in the frequency domain. The deconvolution corrects the seismic records for propagation effects and instrument response. Under the assumption that the focal mechanisms and the depth of the mainshock and the EGF are identical, the deconvolution provides the source time function. The retrieved source time function must have the following physical constraints (Hartzell, 1978; Mueller, 1985): 1) positivity constraint  $s(t) \geq 0$ ; 2) causality  $s(t) = 0$  for  $t \leq 0$ ; 3) finite duration:  $s(t) = 0$  for  $t \geq \tau$ , where  $\tau$  is the duration; and 4) limited frequency band  $S(f) = 0$  for  $f \geq f_c$ , where  $f_c$  is the corner frequency. Negative source time functions have non-physical meaning. This analysis is carried out in paper 1 to study source complexities of the El Mayor-Cucapah earthquake.

### 3.3 Stress drop

Stress drop has an important role in ground motion simulations. Theoretical studies have shown that higher stress drop results in higher ground motion. Stress drop is also important for understanding the physics of the earthquakes. Stress near the faults is non-uniform, but in most applications, we use the stress drop averaged over the fault. Static stress drop is defined as the change in the average state of stress on a fault before and after the rupture. The average stress drop is estimated by  $\Delta\sigma_s = C \mu D/L$ , where  $D$  is the average slip on the fault,  $L$  is a characteristic rupture dimension,  $C$  is a non-dimensional constant that depends on the shape of the rupture surface and on the type of faulting, and  $\mu$  is the rigidity. The strain is  $D/L$ . For circular faults  $L = a$  and  $C = 7\pi/16$ ; for strike slip faults  $L =$



$W$  and  $C = 2/\pi$ ; and for dip slip faults  $L = W$  and  $C = 4(\lambda + \mu)/\pi(\lambda + 2\mu)$ , where  $\lambda$  is the Lamé constant (Kanamori and Anderson, 1975). Stress drop is thought to be independent of the earthquake size (Kanamori and Anderson, 1975).

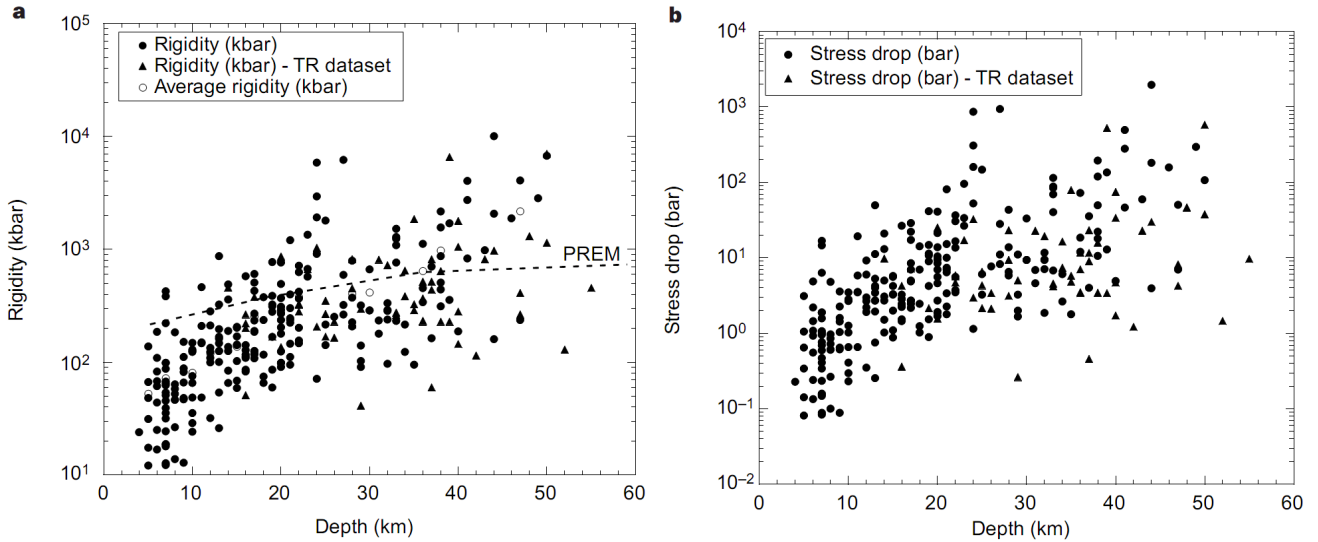


**Figure 5.** a) Rigidity ( $\mu$ ) variation with depth for subduction zone events. b) Stress drop ( $\Delta\sigma_s$ ) variation with depth for subduction zone events (Taken from Bilek and Lay, 1999).

Although seismic moment can be accurately determined, the rupture area is not always determined well. An accurate determination of the fault dimensions is extremely important in determining the stress drop. Fault dimensions can be estimated with geological or seismic methods. As mention in the introduction of section 3, fault dimensions can be obtained from finite-fault models, but slip models generally use fault planes with dimensions exceeding the actual dimensions of the rupture area. In most slip models, heterogeneous slip distribution on the fault can result in regions that have almost zero slip. To accurately estimate fault dimensions from slip models Mai and Beroza (2004) use an autocorrelation width to determine the effective fault dimensions and also normalize the effective mean slip so that the seismic moment of the fault remains unchanged.

Most earthquakes have stress drop in the range 1-10 MPa (Kanamori and Anderson, 1975). In subduction zones, variations with depth of the media properties such as rock density, pressure, temperature, sediment content and other factors control the stress drop (Bilek and Lay, 1999). This results in a great variability of the stress drop values (Figure 5).

### 3.4 Radiated seismic energy

One of the fundamental parameters for describing an earthquake is the radiated seismic energy ( $E_R$ ). Previous studies have reported dependence of the radiated energy with earthquake size (Kanamori and Anderson, 1975) and focal mechanism (e.g. Boatwright and Choy, 1995; Pérez-Campos and Beroza, 2001). Large discrepancy in energy estimations based on different data and techniques for the same earthquake has been observed in many studies. The difficulties in estimating  $E_R$  may arise from the complexity of the seismic source, propagations effect, attenuation and scattering (Kanamori and Brodsky, 2004). In theory, the computation of  $E_R$  simply requires an integration of radiated energy flux. The method adopted here to estimate  $E_R$  is based on Boatwright and Choy (1986). For shallow earthquakes, the radiated energy of the  $P$ -wave group (consisting of  $P$ ,  $pP$  and  $sP$  phases) is related to the energy flux ( $\varepsilon$ ) by

$$E_R^P = 4\pi \langle F^P \rangle^2 (R^P / F^{gP})^2 \varepsilon$$

where  $\varepsilon$  is the  $P$ -wave energy flux,  $\langle F^P \rangle^2$  is the mean-square radiation-pattern coefficient for  $P$  waves;  $R^P$  is the  $P$ -wave geometrical spreading factor;  $F^{gP}$  is the generalized radiation pattern coefficient (Boatwright and Choy, 1986).

$$\varepsilon = \rho \alpha / \pi \int_0^\infty |v(\omega)|^2 e^{\omega t_\alpha} d\omega ,$$

where  $\rho$  is the density,  $\alpha$  is the  $P$ -wave velocity at the receiver; and  $v(\omega)$  is the velocity spectra. The implementation of this method requires that the velocity data

contain spectral information about, above and below the corner frequency of an earthquake. For teleseismically recorded earthquakes, energy is radiated predominantly in the bandwidth 0.01 to about 5.0 Hz (Boatwright and Choy, 1986). Although teleseismic SH and SV wave groups from shallow earthquakes can be analyzed through an extension of these equations, shear waves suffer more attenuation in propagation through the Earth than the  $P$  waves. The loss of seismic signal due to attenuation typically precludes using spectral information for frequencies higher than about 0.2-0.3 Hz for large earthquakes (Boatwright and Choy, 1986). Therefore, it is easier and more accurate to use only the  $P$ -wave group. The final requirement is that we use waveforms that are not complicated by diffractions or secondary phase arrivals. This restricts the usable distance range to stations within the interval of  $30^\circ - 90^\circ$  of the epicenter.

Radiated energy from local and regional records can be computed in a fashion analogous to the teleseismic approach, but  $E_R$  estimates from teleseismic  $P$  waves and regional  $S$  waves can differ by an order of magnitude (Singh and Ordaz, 1994). In this study, the radiated seismic energy ( $E_R$ ) of regional records is estimated following Singh and Ordaz (1994):

$$E_R = \left[ 4\pi R^2 \{G^2(R)/R^2\} \rho \beta / F^2 \right] \int_0^\infty \left\{ V_N^2(f) + V_E^2(f) + V_Z^2(f) \right\} e^{2\pi f R / \beta Q(f)} df ,$$

where  $V_j(f)$  is the velocity spectrum  $j$ th component of the  $S$ -wave group,  $\rho$  is the density,  $\beta$  is the  $S$ -wave velocity,  $R$  is the hypocentral distance, and  $G(R)$  is the geometrical spreading correction,  $F$  is the free-surface amplification,  $Q(f)$  is the quality factor.

Another method to estimate the seismic energy is the empirical Green's function (EGF) technique (Vassiliou and Kanamori, 1982). The method requires the integration of  $f^2 \dot{M}(f)$  up to as large as  $f$  as possible, where  $\dot{M}(f)$  is the moment-rate spectrum of  $S$  wave.  $\dot{M}(f)$  can be obtained from the spectral ratio of

the mainshock and the aftershock recordings (or EGF, defined in section 3.2) and multiplying the ratio by the seismic moment of the aftershock. The radiated seismic energy, is computed using the relation (Vassiliou and Kanamori, 1982)

$$E_R = (4\pi/5 \rho \beta^3) \int_0^{\infty} f^2 \dot{M}(f) df ,$$

where  $\dot{M}(f)$  is the moment rate spectrum,  $\rho$  is the density,  $\beta$  is the  $S$ -wave velocity. For a reliable estimation of  $E_R$ , the corner frequency of the mainshock should be much smaller than the corner frequency of the aftershock. This method has also the advantage that it does not require corrections for attenuation and site effects.

In this study, teleseismic radiated seismic energy estimations are used to develop scaling relationships between  $E_R$  and  $M_w$ .  $E_R$  is also used to analyze energy dependence on focal mechanism for strike-slip events in Baja California and shallow thrust events in the Mexican subduction zone. Regional estimates of  $E_R$  are used to analyze differences in physical properties for near-trench, interplate and normal in-slab events in the Guerrero subduction zone.

### 3.5 Apparent stress ( $\tau_a$ ), $E_R/M_o$ ratio, seismic efficiency ( $\eta_R$ )

The ratio  $E_R/M_o$  has been used in seismology to characterize the dynamic properties of an earthquake (Aki, 1966). The ratio can be interpreted as proportional to the energy radiated per unit fault area and unit of slip ( $E_R/M_o = E_R/\mu DA$ ) (Kanamori and Brodsky, 2004). The ratio depends on many seismogenic properties of the source region so that it varies significantly for earthquakes in different tectonic environments, such as continental crustal, subduction zone, etc (Choy and Boatwright, 1995). Difficulties in determining radiated seismic energy result in wide scatter in the  $E_R/M_o$  ratio (Kanamori and Brodsky, 2004). The radiated energy to seismic moment ratio is different for different types of

earthquakes. For example, tsunami events have the smallest values ( $E_R/M_o < 3 \times 10^{-6}$ ) (Venkataraman and Kanamori, 2004) (Figure 6). As part of this work,  $E_R/M_o$  is used as a discriminant for tsunami events in the Mexican subduction zone.

Apparent stress ( $\tau_a$ ) is defined by  $\tau_a = \mu (E_R/M_o)$ , where  $\mu$  is the rigidity (Wyss and Brune, 1968).  $\tau_a$  does not require the assumption of an specific fault geometry. Boatwright and Choy (1995) discussed the spatial distribution pattern of apparent stress, identifying different stress regimes related to the global tectonics. They found that the highest  $\tau_a$  ( $>3$  MPa) are associated to strike-slip earthquakes, and the lowest  $\tau_a$  ( $< 1.5$  MPa) are associated with thrust earthquakes at subduction zones. In this study, a comparison for  $\tau_a$  in the tectonic areas of Baja California and the Mexican subduction zone is carried out.

The radiation efficiency is defined as the ratio of radiated energy to the sum of the radiated and fracture energy ( $E_G$ ),  $\eta_R = E_R/(E_R + E_G) = 2\mu/\Delta\sigma_s(E_R/M_o)$ , where  $\Delta\sigma_s$  is the static stress drop.  $\eta_R$  is different for different types of earthquakes. Venkataraman and Kanamori (2004) suggest that these differences could be due to differences in their rupture mechanics. The radiation efficiency of most earthquakes lies between 0.25 and 1 (Venkataraman and Kanamori, 2004) (Figure 6). Venkataraman and Kanamori (2004) argue that tsunami earthquakes and some deep earthquakes have small  $\eta_R$  ( $< 0.25$ ) and therefore dissipate a large amount of energy. They suggest that in the case of deep events, energy is probably dissipated as heat, while in the case of the tsunami earthquakes, it is possible that the morphology of the trench causes branching and bifurcation of rupture, resulting large energy dissipation. On the other hand, some earthquakes have  $\eta_R$  larger than 1. This may result from inaccurate estimates of radiated energy and/or stress drops. In this study, a comparison of the radiation efficiency for three different types of earthquakes (near-trench, interplate and normal inslab) in the Guerrero gap area is carried out.

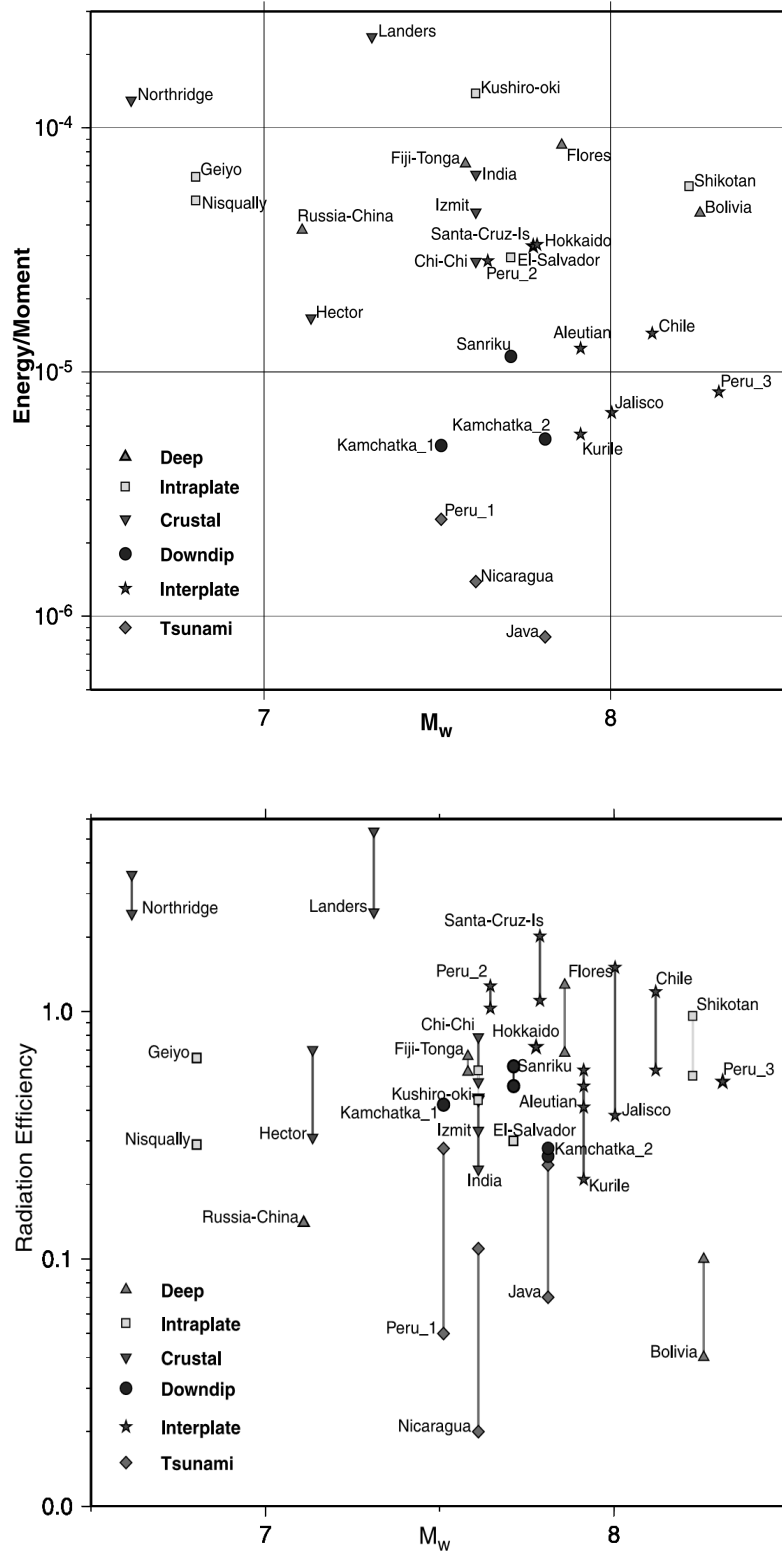


**Figure 6.**  $E_R/M_o$  ratio as a function of magnitude for different type of earthquakes (upper panel). Radiation efficiency as a function of magnitude for different type of earthquakes (lower panel) (Taken from Venkataraman and Kanamori, 2004).

### 3.6 Seismic scaling relationships

Seismic scaling relationships relate one parameter to another. Source scaling relationships not only provide an insight into the mechanics of the rupture process but also give parameters for ground motion prediction for hazard mitigation. In this section, a description of the theoretical basis for source scaling for rupture fault dimensions, average displacement, duration and radiated seismic energy is given.

*Moment versus area.* The scaling relation between  $M_o$  and the rupture area ( $S$ ) is linear and has the following form  $M_o \propto S^{3/2}$ . The linearity of this relation is usually explained in terms of constant  $\Delta\sigma$ . Constant rigidity implies constant stress drop. For the case of a circular fault,  $M_o = \mu DS = (16/7)\Delta\sigma a^3 = (16\Delta\sigma/7\pi^{3/2})S^{3/2}$ , where  $a$  is the radius. This expression can be presented as:  $\log M_o = 3/2 \log S + (16\Delta\sigma/7\pi^{3/2})$ . Thus for a constant  $\Delta\sigma$ ,  $\log S \sim 2/3 \log M_o$ .

*Moment versus length.* For small earthquakes, the relation between  $M_o$  and the rupture length ( $L$ ) is linear and has the form  $M_o \propto L^3$ , under the assumptions of constant  $\Delta\sigma$  and circular fault geometry ( $a = L$ ).  $M_o = \mu DS = (16/7)\Delta\sigma a^3 \approx \Delta\sigma L^3$  or in the logarithmic form  $\log L \sim 1/3 \log M_o$ .

Two rupture length scaling models have been proposed for large events when  $L > W$ . The thickness of the seismogenic zone saturates and the rupture grows along the length direction only. Changes in the scaling relations from small to large earthquakes are expected.

Romanowicz (1992) provided the following relation  $M_o \propto L$  ( $W$  model) for very large earthquakes, suggesting that mean slip and stress drop are related to fault

width, not fault length. Under the assumptions of  $L \gg W$  and  $M_o = \mu DS = \mu DLW$ , which results in the relation  $M_o \propto L$ .

On the other hand, Scholz (1982) provided the following relation  $M_o \propto L^2$  ( $L$  model) for large earthquakes, suggesting that mean slip and stress drop are determined by the rupture length. For large earthquakes,  $L > W$  and  $M_o = \mu DS = \mu DLW$ , which results in the relation  $M_o \propto L^2$ .

No consensus has been reached on whether the scaling relation for  $L$  for large earthquakes should be  $M_o \propto L^2$  or  $M_o \propto L$ .

*Self-similarity conditions.* Kanamori and Anderson (1975) introduced the similarity conditions with the assumption of constant stress drop one gets that  $W/L = k_1$  (constant aspect ratio) and  $D/L = k_2$  (constant strain). Scaling relationships that obey self-similarity should scale like  $M_o \propto L^3$ ,  $M_o \propto W^3$ , and  $M_o \propto D^3$  with the equivalent logarithmic relations of  $\log L \sim 1/3 \log M_o$ ,  $\log W \sim 1/3 \log M_o$ , and  $\log D \sim 1/3 \log M_o$ , respectively. The incorporation of  $M_w$  in the previous equations leads to a linear models  $\log(X) = a + b M_w$ , with  $b = 0.5$  for  $L$ ,  $W$ , and  $D$ . This means that the slope  $b = 0.5$  is an indicator of self-similarity for these relations.

*Scaling for asperity areas.* Quantitative estimation of the size and slip of the asperities is important to source modeling for ground motion prediction. The scaling relations for the asperity area ( $S_a$ ) and the mean slip on the asperities ( $D_a$ ) and  $M_o$  are as follows  $M_o \propto S_a^{3/2}$  and  $M_o \propto D_a^3$ , respectively (Somerville *et al.*, 1999).



*Moment versus radiated seismic energy.* The relation between  $E_R$  and  $M_o$  and  $M_w$  are given by  $\log E_R = \log M_o - 4.3$  and  $\log E_R = 1.5 M_w + 4.8$ , with  $M_o$  and  $E_R$  in Nm (Kanamori and Anderson, 1975). This relation is derived under the assumption of a stress drop of 5 MPa and  $\mu = 50\,000$  MPa. This relation is strictly valid only for earthquakes with the same stress drop, but is a good general model.

*Moment versus source duration.* Previous studies (e.g. Furumoto and Nakanishi, 1983) have shown that the relation between  $M_o$  and the duration ( $\tau$ ) is  $M_o \propto \tau^3$ .

Empirical scaling relationships are developed using source parameters compiled from many earthquakes. Therefore, the empirical scaling relationships differ from the theoretical ones and it is important to develop scaling relations for specific regions. In this study, scaling relationships for rupture fault dimensions ( $W$ ,  $L$  and  $A$ ), duration, average displacement, maximum displacement versus moment magnitude are developed. Fault dimensions are obtained from finite-fault models using the effective dimension criteria (Mai and Beroza, 2000). Additionally, asperities of the slip distributions are characterized obtaining scaling relationships for the combined asperity area of asperities ( $A_a$ ) versus  $M_w$ . The hypothesis of self-similarity is evaluated for  $L$ ,  $W$ , and  $A$ . Scaling relationships for radiated seismic energy are also obtained.

### 3.7 Iterative deconvolution moment tensor inversion

Focal mechanism and seismic moment for a given earthquake are obtained with the moment tensor inversion. Both parameters are important for understanding seismic source and tectonic processes. Estimating the focal mechanism is important because the radiated energy depends on the earthquake type. Moment tensor ( $M_{ij}$ ) provides a complete description of the equivalent body forces of a

seismic point source. The seismic source is described by 6 independent components of the moment tensor. The displacement of the radiated waves can be expressed as a convolution of the moment tensor with the space derivatives of the Green's functions  $G_{ki,j}$ , as  $u_k(\mathbf{x}, t) = M_{ij}(\mathbf{x}, t) * G_{ki,j}$ , where  $M_{ij}(\mathbf{x}, t) = m_{ij}f(t)$ , and  $f$  is the source time function. The Green's function represents the impulse response of the medium between source and receiver, and it contains wave propagation information through the medium from the source to the receiver. The moment tensor inversion solves the following matrix equation:  $\mathbf{u} = \mathbf{G} \mathbf{m}$ , where  $\mathbf{u}$  is a vector containing the seismograms at various stations, the vector  $\mathbf{m}$  contains the moment tensor components, and  $\mathbf{G}$  is a matrix containing the Green's functions. The matrix equation can be solved in the time or in the frequency domain. A variety of methods exist to calculate the moment tensor inversion in both domains (e.g. Hartzell and Heaton, 1983; Ji *et al.*, 2002).

Among the methods, two methods are commonly used, the wavelet domain inversion (Ji *et al.*, 2002) used by the USGS; and the iterative deconvolution method (Kikuchi and Kanamori, 1991) used by the Earthquake Research Institute in Japan. The wavelet domain inversion simultaneously consider both the time and frequency characteristics of the wave-forms. The iterative deconvolution method performs the inversion in time domain. In this study, the iterative deconvolution method is used to estimate the focal mechanism, seismic moment and slip distributions.

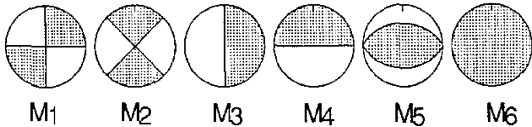
In the iterative deconvolution method, the seismic source is described as a sequence of subevents, each specified by a moment tensor and its onset time and location. The point sources are determined iteratively by matching the observed records and the synthetic seismograms. An arbitrary moment tensor can be

represented as a linear combination of 6 elementary moment tensors  $M_n$  (Figure 7) given by

$$M_{ij} = \sum_{n=1}^{N_e} a_n M_n,$$

The tensors  $M_1$  and  $M_2$  represent pure strike-slip faults; the tensors  $M_3$  and  $M_4$  represent dip-slip faults on vertical planes striking N-S and E-W, respectively. The tensor  $M_5$  represents a 45° dip-slip fault. The tensor  $M_6$  represents an isotropic source radiating energy equally into all directions (explosion or implosion). A deviatoric stress tensor is defined by removing the effect of the compressive stress component. The deviatoric moment tensor is entirely represented by the five elementary moment tensors  $M_1$  to  $M_5$  (Figure 7).

$$\mathbf{M}_1: \begin{bmatrix} 0 & 1 & 0 \\ 1 & 0 & 0 \\ 0 & 0 & 0 \end{bmatrix}; \mathbf{M}_2: \begin{bmatrix} 1 & 0 & 0 \\ 0 & -1 & 0 \\ 0 & 0 & 0 \end{bmatrix}; \mathbf{M}_3: \begin{bmatrix} 0 & 0 & 0 \\ 0 & 0 & 1 \\ 0 & 1 & 0 \end{bmatrix};$$

$$\mathbf{M}_4: \begin{bmatrix} 0 & 0 & 1 \\ 0 & 0 & 0 \\ 1 & 0 & 0 \end{bmatrix}; \mathbf{M}_5: \begin{bmatrix} -1 & 0 & 0 \\ 0 & 0 & 0 \\ 0 & 0 & 1 \end{bmatrix}; \mathbf{M}_6: \begin{bmatrix} 1 & 0 & 0 \\ 0 & 1 & 0 \\ 0 & 0 & 1 \end{bmatrix};$$


**Figure 7.** Elementary moment tensors used in the iterative deconvolution method. (Taken from Kikuchi and Kanamori, 1991).

Following Kikuchi and Kanamori (1991),  $w_{jp}(t; p)$  denotes the Green's function at a station in response to the elementary moment  $M_n$ ,  $x_j(t)$  is the observed record,  $p$  is a parameter that collectively represents the onset time and the location of the subevent. The best estimate for the coefficients  $a_n$  and the parameter  $p$  is obtained

from the condition that the difference between observed and synthetic displacement functions is minimized:

$$\Delta = \sum_{j=1}^{N_s} \int \left[ x_j(t) - \sum_{n=1}^{N_b} a_n w_{jn}(t;p) \right]^2 dt = \text{minimum},$$

where  $N_b$  is the number of elementary moment tensors, and  $N_s$  is the number records used. Once the focal mechanism is obtained from the moment tensor inversion, the method is used to determine the slip distribution. To express the rupture process as a spatial and temporal slip distribution, the fault plane is divided into many subfaults and the slip is estimated at each subfault. The representation theorem (Aki and Richards, 1980) gives the description of the slip on a fault

$$u(x,t) = \iint_{\Sigma} \dot{D}(x,t) * G(x,t) d\Sigma d\tau,$$

where  $u$  is a component of the displacement,  $\dot{D}$  is the slip rate on the fault,  $G$  is the Green's functions. This equation is linearized and solved in a similar form as in the case of the moment tensor inversion. The result of the inversion is the spatial slip distribution and the moment rate function  $\dot{M}(t)$ .

Slip distributions are crucial for an understanding of the rupture process but also to predict strong ground motion of large earthquakes. The rupture patterns on the slip distributions are generally complex and show asperities or regions with higher slip and larger stress drop than the background area. Many studies suggest the

importance of asperities in various seismological problems, such as the nature of ground motion (Das and Aki, 1977), foreshocks (Jones and Molnar, 1979), seismicity patterns (Kanamori, 1981) and regional variation of rupture mode (Lay and Kanamori, 1981). In this work, slip distributions are used to analyze the source process in Mexico. Source parameters from these models are used to develop scaling relationships. Slip distributions are also used to model ground motion with the finite-fault stochastic method.

### 3.8 Ground-motion parameters

From ground motion records various parameters can be derived that are commonly used in earthquake engineering. The simplest and most common parameter is the peak ground acceleration (PGA), which is the largest absolute value of acceleration. Similarly, the values of the peak ground velocity (PGV) and displacement (PGD) are used to characterize the ground motion. For engineering applications, the most important representation of the ground motion is the response spectrum. The response spectrum is a plot of the maximum response experienced by a group of single-degree-of-freedom (SDOF) oscillators under seismic excitation (Figure 8). This can also be represented as a pendulum described by its natural period of vibration ( $T_n$ ) and its damping ( $\xi$ ). In earthquake engineering, a damping value of 5 % is commonly used. Acceleration response is used to calculate the lateral force exerted on the structures during an earthquake by multiplying it with the mass of the building. The pseudo spectral acceleration (PSA) is defined as  $PSA = (2\pi/T_n)^2 SD$ , where  $SD$  is the spectral displacement. In this work, ground motion parameters (PGA, PGV and PSA) for near-trench and inslab earthquakes are estimated in order to derive ground-motion attenuation relationships. These relations are obtained with the one-stage maximum-likelihood method explained in the next section.

### 3.9 Ground-motion attenuation relationships

The development of ground-motion attenuation relationships is very important for seismic hazard analysis for earthquake hazard mitigation. These relations are empirically derived from strong-motion records, and they are used to estimate ground-motion values for an earthquake given the magnitude, distance, soil conditions, etc. Ground-motion attenuation relationships mathematically represents multivariate regressions and can be solved with different methods. First, a functional form is proposed based on the knowledge of the data. There are many models in the literature but the most representative functional form of the ground-motion attenuation relationships is given by

$$\log Y = c_1 + c_2 M - c_3 \log R + c_4 R + c_5 H + c_6 F + c_7 S + \varepsilon,$$

where  $Y$  is a ground parameter (PGA, PGV, or PSA at specific frequencies),  $M$  is the magnitude;  $R$  is a measure of the distance approximately equal to the average distance to the fault surface  $R = (D_{\text{fault}}^2 + h^2)^{0.5}$ , where  $D_{\text{fault}}$  is the shortest distance from the site to the source (either point-source or finite-fault source distance);  $H$  is the hypocenter depth;  $F$  is the faulting mechanism,  $S$  is the local site condition (usually  $S = 1$  for rock sites and  $S = 0$  for soil sites), and  $\varepsilon$  is a random error term. The term  $\log Y \propto c_2 M$  is consistent with the original definition of magnitude; the term  $\log Y \propto -c_3 \log R$  is consistent with the geometric attenuation; and the term  $\log Y \propto c_4 R$  is consistent with the anelastic attenuation. These equations are simple models for a very complex phenomenon so large scatter is observed between the fitted curves and the observations. The residual between the predicted values  $\hat{Y}_i$  and the observations  $Y_i$  is given by  $R = \log(Y_i / \hat{Y}_i)$ .

One important parameter in developing ground-motion attenuation relationships is the distance between the source and the seismic stations. There are two types of source-to-site distances: single point and finite-fault distances. Examples of point-source distances are the epicentral distance ( $r_{epi}$ ) and the hypocentral distance ( $r_{hypo}$ ). For earthquakes with large rupture areas  $r_{epi}$  and  $r_{hypo}$  are poor measures of distance, but they are used for characterizing distance of small events. In the case of the finite-fault distances, the most common distances are: the closest horizontal distance to the vertical projection of the rupture plane ( $r_{jb}$ ) (Joyner and Boore, 1981) (Figure 9); the closest distance to the rupture plane ( $r_{rup}$ ) (Schnabel and Seed, 1973) (Figure 9); and the closest distance to the seismogenic part of the rupture plane ( $r_{seis}$ ) (Campbell, 1987) (Figure 9). In Figure 9 different distance measures for vertical and dipping faults are shown.

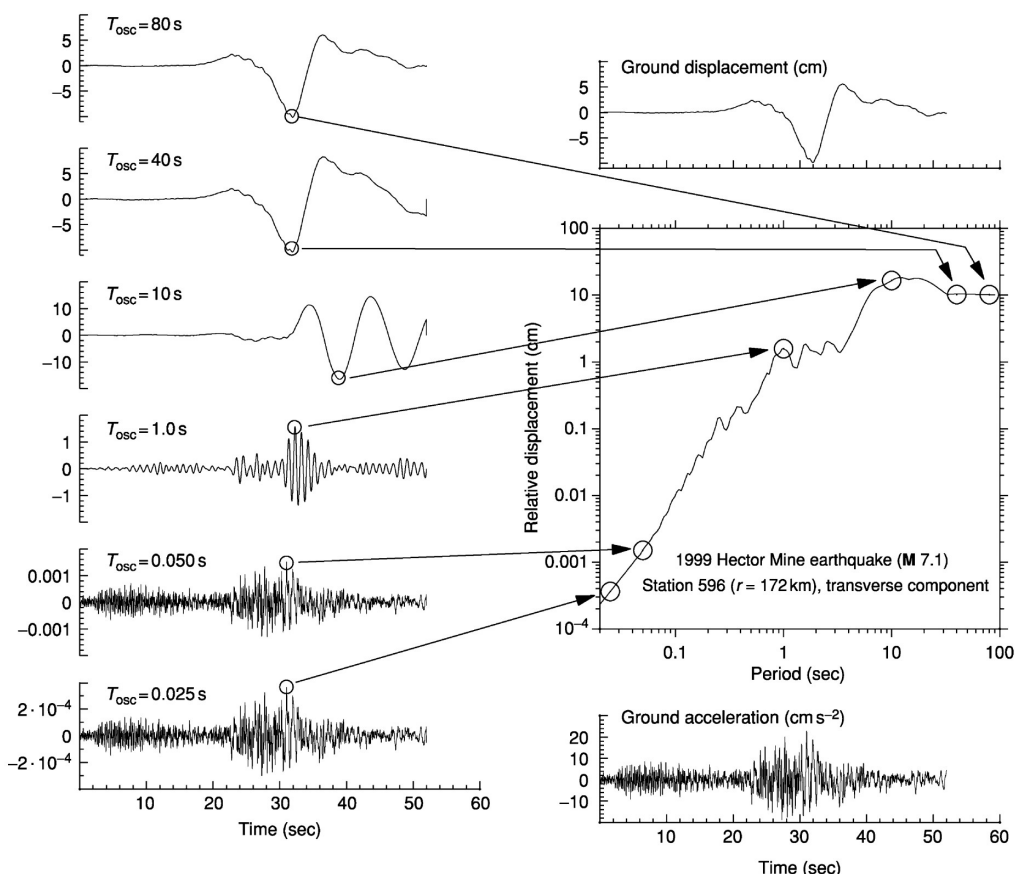


**Figure 8.** Response spectrum definition. Displacement response for simple oscillators with different natural period (left side). Plot of the maximum displacement versus natural period (displacement response spectrum) (right side) (Taken from Bommer and Boore, 2004).

Many methods have been developed for multivariate regression analysis in ground motion analysis. Some of them are the least-squares method, the multivariate Bayesian method (Arroyo and Ordaz, 2010a, 2010b), the one-stage maximum-likelihood method (Joyner and Boore, 1993, 1994), and the two stage weighted least-squares regression (Joyner and Boore, 1993). Joyner and Boore (1993) studied how the one-stage maximum-likelihood method and the two stage method are related; they found that both methods lead essentially to the same results. The one-stage maximum-likelihood method is adopted for comparisons with the results obtained by Garcia *et al.* (2005) for inslab events in central Mexico. For purposes of the thesis, the discussion focuses on the one-stage maximum-likelihood method.

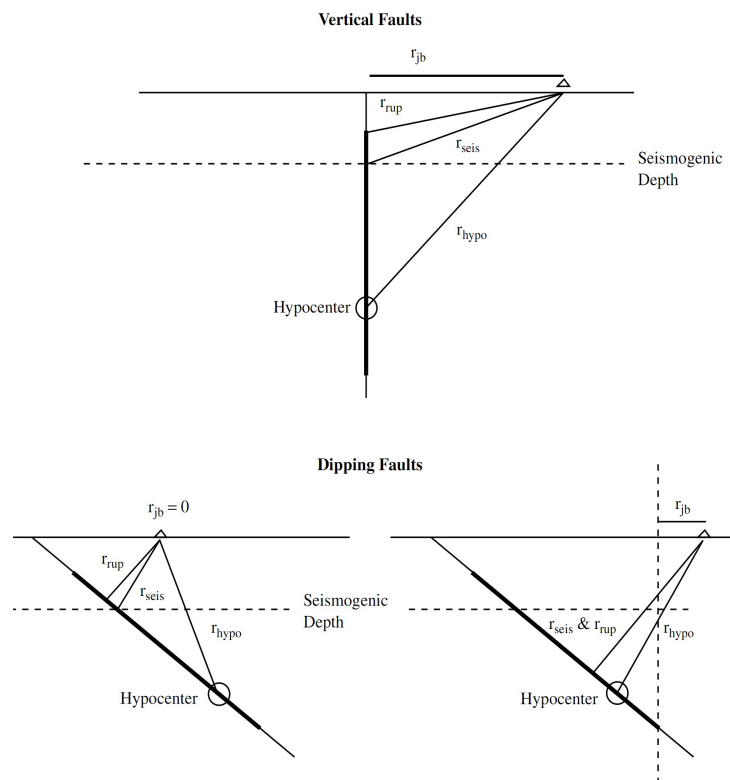


**Figure 9.** Different distance definitions (Taken from Campbell, 2003).

The method was initially introduced by Brillinger and Preisler (1984), then improved by Abrahamson and Youngs (1992), and later re-examined by Joyner and Boore (1993, 1994). In this method, the error is partitioned into two parts,



intra- and interevent errors ( $\varepsilon_e$  and  $\varepsilon_r$ , respectively). All parameters are determined simultaneously by inverting the matrix form of the ground-motion attenuation relationship:  $\mathbf{Y} = \mathbf{X}\mathbf{B} + \mathbf{e}$ , where  $\mathbf{B}$  is the vector of the coefficients ( $c_i$ ),  $\mathbf{X}$  is a data matrix, and  $\mathbf{e}$  is the error vector composed by  $\varepsilon_e$  and  $\varepsilon_r$ . Under the assumption that the errors are uncorrelated, normally distributed with zero means, and with constant variances ( $\sigma_e$  and  $\sigma_r$ ), the solution of the system is given by  $\hat{\mathbf{B}} = (\mathbf{X}^T \mathbf{V}^{-1} \mathbf{X})^{-1} \mathbf{X}^T \mathbf{V}^{-1} \mathbf{Y}$ , where  $\mathbf{V}$  is the variance-covariance matrix of  $\mathbf{e}$ . The parameters to be estimated are  $c_i$ ,  $\sigma_e$  and  $\sigma_r$ . The final solution corresponds to the values of  $\mathbf{B}$  and  $\sigma$  that maximize the log-likelihood function ( $\ln L$ ). This solution is found iteratively using a search algorithm (Joyner and Boore, 1993).

### 3.10 The stochastic method

Ground motion simulations for large earthquakes is a crucial problem in seismology and earthquake engineering. Many applications require methods that describe the amplitude, frequency content, and duration of the expected ground motions. The stochastic method provides these information. The stochastic method was introduced by Boore (1983) and is used to simulate high-frequency ground motions ( $f > 1$  Hz). The high-frequency earthquake motions are represented as band-limited Gaussian noise having an  $\omega$ -square mean spectrum. The Fourier amplitude spectrum of the point-source model is given by

$$A(M_o, R, f) = E(M_o, f) P(R, f) Z(f) I(f),$$

where  $M_o$  is the seismic moment,  $E$  is the earthquake source,  $P$  is the path effects,  $Z$  is the site effects, and  $I$  is the instrument response. The most common representation of the source is the  $\omega$ -square model (Aki, 1967), but some other source models have been used in the stochastic model. The scaling of the spectra

is described by the following relation  $M_o f_o^3 = \text{constant}$  (Aki, 1967). The corner frequency is given by  $f_o = 4.9 \times 10^6 \beta (\Delta\sigma/M_o)^{1/3}$ , where  $\beta$  is the shear velocity in km/s,  $\Delta\sigma$  is the stress drop in bars, and  $M_o$  in dyne cm. The source spectra can be expressed by the following equation:  $E(M_o, f) = CM_o S(M_o, f)$ , where  $C$  is a constant and  $S(M_o, f)$  is displacement source spectrum. The constant  $C$  is defined as  $C = R_{\theta\phi} V F / (4\pi\rho\beta^3 R_o)$ , where  $R_{\theta\phi}$  is the radiation pattern (0.55 for shear waves),  $V$  represents the partition of the total shear-wave energy into horizontal components ( $1/\sqrt{2}$ ),  $F$  is the effect of the free surface (2),  $\rho$  is the density, and  $R_o$  is a reference distance, usually set equal to 1 km.

The  $\omega$ -square source model is given by  $S(f) = (2\pi f)^2 / [1 + (f/f_o)^2]$ . Path effects account for geometrical spreading  $G$  and attenuation (intrinsic and scattering attenuation,  $Q$ ),  $P(f) = e^{-\pi f R/Q(f)\beta} G(f)$ . In order to perform reliable ground motion simulations, the site response must be taken into account. In the stochastic method (Boore, 1983, 2003), site effects ( $Z$ ) are described as the combination of site amplification  $A$ , and the near-surface attenuation  $D$ , as  $Z(f) = A(f) D(f)$ , where  $D(f) = e^{-\pi kf}$ . Site amplification occurs due to the seismic impedance effect when waves propagate with lower velocities than the velocity gradient from the source toward the upper layers.

There are several methods in the literature for estimating site amplifications, such as the horizontal to vertical spectral ratios ( $H/V$  ratios) (Nakamura, 1989; Lermo and Chavez-Garcia, 1993). The  $H/V$  ratio technique is based on the observation that the effect of amplification on the vertical component is weaker than the horizontal component. It has been reported that  $H/V$  technique underestimate the amplifications (Castro *et al.*, 2001), but it can be consider as a rough indicator of the soil response. In the stochastic simulations of this work, the  $H/V$  method at a single station is used instead the of the standard reference site method because

none of the events analyzed were recorded close enough at rock and soil sites, which would not allow to use rock sites as reference.

For large earthquakes, finite-fault representation of the source is a better approach to simulate ground motions because it considers the effects of the geometry, slip heterogeneity, and source directivity, which can affect ground motion simulations. The stochastic finite-fault simulation method (Beresnev and Atkinson, 1997) is an extension of the point source stochastic method (Boore, 1983). In this method, the fault plane is divided into small subfaults, and each is represented as a point source with an  $\omega^2$  spectrum. The rupture starts at the hypocenter and propagates until each subfault is triggered. Ground motion from the entire fault is obtained by adding the contributions from all the subfaults with an appropriate delay time. One problem of this approach is the dependence of the total radiated energy on the subfault size; and the constraint on the number of subfaults (Beresnev and Atkinson, 1997). To deal with these difficulties, Motazedian and Atkinson (2005) introduced the dynamic corner frequency approach into the finite-fault stochastic method. The improvements of the dynamic corner frequency approach are that the high-frequency energy radiated is conserved regardless of the subfault size so it can be used to model a broader magnitude range (Motazedian and Atkinson, 2005). In this work, the finite-fault stochastic method is used to model ground motions for normal, thrust and strike-slip events, using the slip distributions obtained with the iterative deconvolution method.

## 4. Results

The results of this thesis are given in four research papers describing the seismic source of earthquakes in Mexico, the development of empirical scaling and ground-motion attenuation relationships. In this section, I present each of the papers with their objectives and relevance, and their main findings and conclusions are summarized.

### 4.1 Stochastic finite-fault ground-motion simulation and source characterization of the 4 April 2010 $M_w$ 7.2 El Mayor-Cucapah earthquake (Paper 1)

Accurate ground motion simulations require to study how earthquakes rupture in detail. Earthquake rupture process is a very complex physical phenomenon, and it is strongly affected by the tectonics. The aim of this paper is to study source complexities of the 4 April 2010  $M_w$  7.2 El Mayor-Cucapah earthquake. As part of this work ground motions are modeled at rock and soil site conditions as well. The results obtained can be used in having a more comprehensive insight of this continental strike-slip event in Baja California. Several techniques were applied in this paper to have a complete analysis. The main findings are: 1) the source time function analysis with the EGF technique reveals that the mainshock consists of at least two subevents. Additionally, the inspection of the near-fault ground motion records show several acceleration peaks. A total rupture duration of the mainshock of about 52 – 60 s was obtained using four different EGFs; 2) the moment tensor inversion shows a right lateral focal mechanism of a strike of  $312^\circ$ , a dip of  $84^\circ$  and a rake of  $-177^\circ$ , with  $M_o = 9.94 \times 10^{19}$  Nm; 3) teleseismic inversion shows two asperities. A rupture area of 140 x 20 km (based on the aftershock distribution) was used in the slip inversion. The obtained slip model agrees with the spatial distribution of the seismicity leading to the following interpretation of the earthquake rupture. First, the rupture nucleated near the hypocenter, breaking

---

bilaterally the first asperity. Second, the rupture stopped in the southeastern part and continued propagating in the northwest direction, breaking unilaterally the large asperity. The total rupture time of the mainshock based on the teleseismic inversion is about 50 – 55 s; 4)  $H/V$  analysis shows that stations located at soil sites in this region show amplifications ranging from 3.4 to 6.0 and predominant frequencies ranging from 1.0 Hz to 4Hz. Stations located at rock sites show no amplification; 5) the finite-fault stochastic results show that a stress drop of 40 bars match best the simulated spectra with the observations. Additionally, the method shows that the selected regional parameters (geometrical spreading, attenuation, and distance-dependence duration empirical model) reproduce reasonably well the shape and duration of the observations.

## 4.2 Finite-fault scaling relation in Mexico (Paper 2)

Empirical scaling relationships provide information about the seismic source. Ideally, they should be derived for specific regions, but in many cases, global models or inappropriate relationships (for different types of earthquakes) are used in many applications. Currently, the developing of source scaling relations for subduction earthquakes has been focused on global data (Blaser *et al.*, 2010; Strasser *et al.*, 2010). Scaling relationships derived from slip distributions provide an insight into the rupture process, but few examples can be found in the literature (Somerville *et al.*, 1999; Mai and Beroza, 2000) based on global data and mixing different types of earthquakes. The first objective of this paper is to develop scaling relationships for shallow thrust subduction zone earthquakes based on finite-fault models. Second, to analyze source parameters from crustal strike-slip events in the Gulf of California area; from thrust interplate earthquakes of the Mexican subduction zone. Third, to characterize the asperities both regions using slip distributions. The main results of this paper are: 1) the development of empirical relationships for estimating fault dimensions, combined asperity area, ratio of combined asperity area to rupture area, maximum displacement, average

displacement, duration, and radiated seismic energy for subduction earthquakes. The obtained relationships show good correlation with the equivalent empirical relations for subduction zone earthquakes. The results also show robust slip solutions and thus reliable source parameter estimates for earthquakes in the magnitude range of 6.5 to 8.0; 2) the results support previous reports of mechanism dependence of the radiated energy and apparent stress (e.g. Choy and Boatwright, 1995; Pérez-Campos and Beroza, 2001). Stress drop also shows different behavior in both regions. The data show that stress drop in the subduction zones is smaller than stress drop on continental and oceanic transform faults in Baja California. The  $E_R/M_o$  ratio varies with the earthquake type. It has been reported that  $E_R/M_o = 3 \times 10^{-6}$  for tsunami earthquakes, the results are successful in identifying some of the reported tsunami events by NOAA. The discrepancies may come from the difficulty of estimating the radiated seismic energy; 3) the ratio of displacement to rupture width suggests a constant stress drop supporting self-similarity for subduction events, while for strike-slip events shows more variability. Additionally, comparisons of the slopes of the regression models for the length, width, and rupture area with their respective theoretical slopes values (0.5 and 1.0 for  $L-W$ , and  $A$ , respectively) suggest self-similarity; 4) The area of the asperities represent an average 20-23% for strike-slip events, and 25% for thrust events of the total rupture area using two different criteria based on average slip (Somerville *et al.*, 1999) and maximum displacement (Mai *et al.*, 2005). Although the asperities are obtained from waveform inversion in a limited frequency range (usually lower than 1 Hz), the source characterization of the asperities provides more reliable information for ground motion simulations.

### 4.3 Source study of three moderate size recent earthquakes in the Guerrero seismic gap and its tectonic implications (Paper 3)

Seismic hazard in the Mexican subduction zone involves mainly three types of earthquakes, interplate, near-trench and normal in-slab events. Paper 4 focuses on

the Guerrero subduction zone in central Mexico, where a seismic gap has been identified. Interplate events are the most common type of earthquakes, and the gap could be filled by an interplate event. The near-trench events could generate tsunami and normal inslab events mostly affect the inland regions of Mexico with high population density. Global seismic source parameter studies have shown differences among the different types of earthquakes (Choy and Boatwright, 1995; Venkataraman and Kanamori, 2004). At regional scale, different behavior of source parameters have been reported (Iglesias *et al.*, 2003; García *et al.*, 2004). The aim of this paper is to analyze source parameters from different types of earthquakes and to compare their effect on ground motions. The studied events are the 15 July 1996 Guerrero near-coast event ( $M_w = 6.6$ ), the 18 April 2002 Guerrero near-trench event ( $M_w = 6.7$ ), and the 11 December 2011 Guerrero inslab event ( $M_w = 6.5$ ). The similarity in seismic magnitude allows the comparison of stress drop, radiated seismic energy,  $E_R/M_o$  ratio, radiation efficiency, and ground motions among the events. Regional and teleseismic data are analyzed, and ground motion simulation is computed with the finite-fault stochastic method. The main results can be summarized as: 1) From moment tensor inversion, the obtained focal mechanisms are: (297, 21, 93) with  $M_o = 1.54 \times 10^{19}$  Nm, (291, 21, 89) with  $M_o = 1.68 \times 10^{19}$  Nm, and (288, 39, -82) with  $M_o = 1.54 \times 10^{19}$  Nm for the near-coast, near-trench and inslab event, respectively; 2) The slip distributions show one asperity for all the events. The asperity area represents 24% of the total rupture area for both the near-coast and near-trench events, and 18% for the case of the inslab event. The inversion also shows that near-trench event has the lowest rupture velocity, and thus the longest duration; 3) the calculated static stress drop based modeled fault geometry is 0.71, 0.88, and 3.05 MPa for the near-coast, near-trench and inslab event, respectively. The results agree with the stress drop depth variation in subduction zones reported by Bilek and Lay (1999); 4) the radiated energy estimates based on teleseismic data show that the near-trench event has the lowest energy. The results for  $E_R/M_o$  ratio are  $1.64 \times 10^{-6}$ ,  $3.40 \times 10^{-6}$ , and  $7.51 \times 10^{-6}$  for the near-trench, near-coast, and inslab events, respectively. The near-trench event has a  $E_R/M_o$  ratio  $< 3 \times 10^{-6}$ , and it is identified as a slow

event. By comparing the radiation efficiency ( $\eta_{inslab} < \eta_{interplate} < \eta_{near-trench}$ ), it is observed that the inslab event has the most efficient rupture mechanics; 5) Observations of peak ground acceleration reflect differences in source parameters and stress drop controls the ground motion level. Near-trench events in the Mexican subduction zone have anomalous low peak accelerations (Iglesias *et al.*, 2003). The stochastic simulations show that the peak ground accelerations can be explained by a stress drop of 0.38, 3.40, and 34.20 MPa for the near-trench, near-coast, and inslab events, respectively, which is the expected behavior for the stress drop ( $\Delta\sigma_{near-trench} < \Delta\sigma_{interplate} < \Delta\sigma_{inslab}$ ) in subduction zones.

#### 4.4 Ground-motion attenuation relationships for near-trench and normal-faulting inslab subduction zone earthquakes in Mexico (Paper 4)

The ground motion level varies according to the earthquake type, reflecting differences in source parameters, such as stress drop. Ground motions from normal-faulting inslab events are larger than those for interplate and near-trench events. Ground motions of near-trench events in Mexico are weak along the coast and inland areas, but hazard arises if they can generate a tsunami. The difference in ground motions of inslab and near-trench highlights the importance of developing specific ground-motion attenuation relationships for different types of earthquakes. No specific ground-motion relations for near-trench events in central Mexico and for normal-faulting inslab events in southern Mexico had been developed so far this constitutes the main issue in paper 4. The near-trench events consist of 17 earthquakes ( $4.4 \leq M_w \leq 7.1$ ) and the inslab events of 25 intermediate-depth events ( $5.0 \leq M_w \leq 7.2$ ; and  $32.2 \leq H \leq 198$  km). The relations are developed for PGV, PGA, 5% damping PSA response spectra at 15 frequencies. The relationships are estimated with the one-stage maximum likelihood method (Joyner and Boore, 1993, 1994) after analyzing different functional forms for the regression. The relation for near-trench events predicts ground motions as expected, lower than interplate and inslab events. A



comparison between inslab events in Guerrero and southern Mexico is carried out. The results suggest that the events in southern Mexico decay somewhat faster than the events in the central region. Ray trajectories crossing the mantle have been proposed by other authors to explain this observation. Predicted values from this study are in reasonable agreement with other relationships (Fukushima and Tanaka, 1990; Atkinson and Boore, 2003; García *et al.*, 2005).

## 5. Conclusions and future perspectives

This study contains novel scaling and ground-motion relationships and provides new information about the source parameters for different types of earthquakes. The study highlights the importance of source studies on ground motion simulations. This work tackles these topics using different methodologies and data. The conclusions can be summarized as:

- The EGF technique is effective in analyzing source complexities such as directivity effect and identifying subevents. The reliability of the results depends on the number and azimuthal cover of the stations.
- Although the  $H/V$  technique at single station underestimate the amplifications, it is successful in determining the predominant frequencies. Teleseismic slip distributions and  $H/V$  technique together with the finite-fault stochastic method provides an effective and fast methodology to calculate ground motions.
- Scaling relationships derived from slip distributions provide an insight into the rupture process. The asperity characterization shows that 1) asperities represent 22% and 24% of the total rupture area for strike-slip and thrust events; 2) for all the events analyzed ( $6.5 < M_w < 8.0$ ), the total number of asperities varies between 1 and 2; and 3) asperities have larger stress drop than background areas. Source parameters on asperities scale with moment magnitude.

- The obtained regression models suggest self-similarity for subduction zone events with magnitudes between 6.5 and 8.0. The results cannot clarify the issue of possible self-similarity scaling for small events and large events ( $M > 8$ ). This issue is an ongoing controversial topic in seismology. The obtained relationships show good correlation with the equivalent empirical relations for other authors.
- Source parameters exhibit mechanism dependence, strike-slip events have higher apparent stress and radiated energy than shallow thrust interplate subduction zone events. Stress drop in the subduction zone is smaller than stress drop on continental and oceanic transform faults. In the Guerrero subduction zone, the analyzed events suggest that near-trench events have the lowest radiated seismic energy. Near-trench events are expected to have the lowest values of  $E_R/M_o$  and the highest values should correspond to the inslab events. Stress drop varies with depth according to  $\Delta\sigma_{\text{near-trench}} < \Delta\sigma_{\text{interplate}} < \Delta\sigma_{\text{inslab}}$ . Inslab event has the most efficient rupture mechanics.
- Comparison of the obtained predicted ground motion curve for normal-faulting inslab in southern Mexico and the one obtained for central Mexico, suggests that events in southern Mexico decay somewhat faster than events in the central region. This study confirms that ground motions predicted by near-trench attenuation models are lower than those predicted by normal inslab and interplate models, as expected.

## 5.1 Future perspectives

The study of the seismic source is a very active area in earthquake seismology. Specific suggestions for future work regarding ground motion simulation, finite-

fault scaling and ground-motion attenuation relationships are given in the following section.

Detailed studies are needed to improve the ground motion prediction. The stochastic method requires knowledge of many parameters that describe the seismic source, wave path and site effects which depends on the study area. It is necessary to conduct more studies about source spectra, attenuation and site effects. For example, some studies have shown that inslab events have source spectra that differ from the classical Brune model (for example with two corner frequencies as reported by Garcia *et al.*, (2004) for central Mexico). It highlights the possibility that source spectra vary with the type of earthquake. Another example is the attenuation for near-trench and inslab events. Attenuation in southern Mexico is poorly studied and it is needed to study source parameters of inslab earthquakes.

The main limitation of the finite-fault scaling is the reduced number of slip-distributions. With time more solutions will be available and the presented scaling relationships can be refined. The methodology can also be applied to right-lateral events in Baja California making possible the development of scaling relations for continental and oceanic strike-slip events; to shallow normal inslab events, and to normal intermediate-depth earthquakes. These relations will be important to understand the source process from different types of earthquakes and to assess the seismic hazard.

From the seismological perspective, more robust finite-fault models derived from both seismic and geodetic data (GPS and/or InSAR) are needed. It is also important to incorporate local and regional seismic data, which allows to develop new relations such as the relation between the flat level of the acceleration

spectrum and seismic moment. This relation has important implications for strong ground motion prediction.

It is also important to compare the obtained ground-motion attenuation relationships with relations obtained with other methods such as the multivariate Bayesian methods and the non parametric method. Stable models should show good correlation among the methods. Another important point is the reevaluation of these relations when more data with high quality is available.

## References

- Abrahamson, N. A., and R. R. Youngs (1992). A stable algorithm for regression analysis using the random effects model, *Bull. Seism. Soc. Am.* **82**, 505-510.
- Aki, K. (1967). Scaling law of seismic spectrum, *J. Geophys. Res.* **72**, 1217-1231.
- Arroyo, D. and M. Ordaz (2010a). Multivariate Bayesian regression analysis applied to ground-motion prediction equations, part 1: theory and synthetic example, *Bull. Seism. Soc. Am.* **100**, 1551-1567.
- Arroyo, D. and M. Ordaz (2010b). Multivariate Bayesian regression analysis applied to ground-motion prediction equations, part 2: Numerical example with actual data, *Bull. Seism. Soc. Am.* **100**, 1568-1577.
- Astiz, L., and H. Kanamori (1984). An earthquake doublet in Ometepec, Guerrero, Mexico, *Phys. Earth Planetary Int.*, **34**, 24-45.
- Atkinson, G. M., and D. M. Boore (2003). Empirical ground-motion relations for subduction-zone earthquakes and their application to Cascadia and other regions, *Bull. Seism. Soc. Am.* **93**, 1703-1729.
- Beresnev, I. A., and G. M. Atkinson (1997). Modeling finite-fault radiation from the  $\omega^n$  spectrum, *Bull. Seism. Soc. Am.* **87**, 67-84.
- Bilek, S. L., and T. Lay (1999). Rigidity variations with depth along interplate megathrust faults in subduction zones, *Nature* **400**, 443-446.
- Blaser, L., F. Krüger, M. Ohrnberger M., and F. Scherbaum (2010). Scaling relations of earthquake source parameter estimates with special focus on subduction environment, *Bull. Seism. Soc. Am.* **100**, 2914-2926.

Boatwright, J., and G. L. Choy (1986). Teleseismic estimates of the energy radiated by shallow earthquakes, *J. Geophys. Res.* **91**, 2095-2112.

Bommer, J. J., and D. M. Boore (2004). Engineering Seismology, a chapter in *Encyclopaedia of Geology*, 499-515.

Boore, D. (1983). Stochastic simulation of high-frequency ground motions based on seismological models of the radiated spectra, *Bull. Seism. Soc. Am.* **73**, 1865-1894.

Boore, D. M. (2003). Simulation of ground motion using the stochastic method, *Pure and Applied Geophysics* **160**, 635-675.

Bravo, H., C. J. Rebolgar, A. Uribe, and O. Jimenez (2004). Geometry and state of stress of the Wadati-Benioff zone in the Gulf of Tehuantepec, Mexico, *J. Geophys. Res.*, **109**, B04307, doi:10.1029/2003JB002854.

Brillinger, D. R., and H. K. Preisler (1984). An exploratory analysis of the Joyner-Boore attenuation data, *Bull. Seism. Soc. Am.* **74**, 1441-1450.

Campbell, K. W. (1987). Predicting strong ground motion in Utah, in *Assessment of regional earthquakes hazards and risk along the Wasatch Front, Utah*, Vol. II, P.L. Gori and W. W. Hays, Eds., U.S. Geological Survey, Open-File Rept. 87-585 pp L1-L90.

Campbell K. W. (2003). Engineering models of strong ground motion in *Earthquake engineering handbook* Wai-Fah Chen and Charles Scawthorn (Editors), CRC Press, Chapter 5.

Castro, R. R., A. Rovelli, M. Coco, M. Di. Bona, and F. Pacor (2001). Stochastic simulation of strong-motion records from the 26 September

Choy, G.L., and J. Boatwright (1995). Global patterns of radiated seismic energy and apparent stress, *J. Geophys. Res.* **100**, 18,205-18,228.

Das, S. and K. Aki (1977). Fault plane with barriers a versatile earthquake model, *J. Geophys. Res.* **82**, 5658-5670.

DeMets, C., R. Gordon, D. Argus, and S. Stein (1994). Effect of recent revisions to the geomagnetic reversal time scale on estimates of current plate motions, *Geophys. Res. Lett.*, **21**, 2191-2194.

DeMets, C. (1995). A reappraisal of seafloor spreading lineations in the Gulf of California: Implications for the transfer of Baja California to the Pacific plate and estimates of Pacific-North America motion, *Geophys. Res. Lett.*, **22**, 3545-3548.

Currie, C. A., R. D. Hyndman, K. Wang, and V. Kostoglodov (2001). Thermal models of the Mexican subduction zone: implications for the megathrust seismogenic zone, *J. Geophys. Res.* **107**, B12, doi:10.1029/2001JB000886.

Fukushima, Y., and T. Tanaka (1990). A new attenuation relation for peak horizontal acceleration of strong earthquake ground motion, *Bull. Seism. Soc. Am.* **80**, 757-783.

Furumoto, M., and I. Nakanishi (1983). Source times and scaling relations of large earthquakes, *J. Geophys. Res.* **88**, 2191-2198.

García, D., S. K. Singh, M. Herráiz, J. F. Pacheco, and M. Ordaz (2004). Inslab earthquakes of central Mexico:  $Q$ , source spectra, and stress drop, *Bull. Seism. Soc. Am.* **94**, 789-802.

García, D., S. K. Singh, M. Herráiz, M. Ordaz, and J. F. Pacheco (2004). Inslab earthquakes of central Mexico: peak ground-motion parameters and response spectra, *Bull. Seism. Soc. Am.* **95**, 2272-2282.

Goff, J. A., E. A. Bergman, and S. C. Solomon (1987). Earthquake source mechanisms and transform fault tectonics in the Gulf of California, *J. Geophys. Res.*, **92**, 10,485-10,510.



Hartzell, S. H. (1978). Earthquake aftershocks as Green's functions, *Geophys. Res. Lett.*, **5**, 1-4.

Iglesias, A., S. K. Singh, J. F. Pacheco, L. Alcántara, M. Ortiz, and M. Ordaz (2003). Near-trench Mexican earthquakes have anomalously low peak acceleration, *Bull. Seism. Soc. Am.* **93**, 953-959.

Jennings, C. W. (1994). *Fault Activity Map of California and Adjacent Areas with Location and Ages of Recent Volcanic Eruptions*. California Geologic Data Map Series, map no. 6. California Division of Mines and Geology.

Jonas, L. M. and P. Molnar (1979). Some characteristics of foreshocks and their possible relationship to earthquake prediction and premonitory slip on faults, *J. Geophys. Res.* **84**, 3596-3608.

Joyner, W. B., and D. M. Boore (1981). Peak horizontal acceleration and velocity from strong-motion records including records from the 1979 Imperial Valley, California, earthquake, *Bull. Seism. Soc. Am.* **71**, 2011-2038.

Joyner, W. B., and D. M. Boore (1993). Methods for regression analysis of strong-motion data, *Bull. Seism. Soc. Am.* **83**, 469-487.

Joyner, W. B., and D. M. Boore (1994). Errata: Methods for regression analysis of strong-motion data, *Bull. Seism. Soc. Am.* **84**, 955-956.

Kanamori, H., and D. L. Anderson (1975). Theoretical basis of some empirical relations in seismology, *Bull. Seism. Soc. Am.*, **65**, 1073-1095.

Kanamori H. (1981). The nature of seismicity patterns before large earthquakes, in *Earthquake Prediction*, D. W. Simpson and P. G. Richards, Editors, American Geophysical Union, Washington, D. C., 1-19.

Kanamori, H., and E. E. Brodsky (2004). The physics of earthquakes, *Rep. Prog. Phys.* **67** 1429-1492.

Kikuchi, M., and H. Kanamori (1982). Inversion of complex body waves, *Bull. Seism. Soc. Am.*, **72**, 491-506.

Kikuchi, M., and H. Kanamori (1986). Inversion of complex body waves-II, *Phys. Earth Planetary Int.*, **43**, 205-22.

Kikuchi, M., and H. Kanamori (1991). Inversion of complex body waves-III, *Bull. Seism. Soc. Am.*, **81**, 2335-2350.

Kostoglodov, V., and Pacheco, F. J. (1999). 100 years of seismicity in Mexico, *Instituto de Geofísica, UNAM* (poster).

Kostoglodov, V., S. K. Singh, J. A. Santiago, K. M. Larson, A. R. Lowry, and R. Bilham (2003). A large silent earthquake in the Guerrero seismic gap, Mexico, *Geophys. Res. Lett.* **15**, doi:10.1029/2003GL017219.

Larson, K. M., V Kostoglodov, M. Shin'ichi, and J. A. Santiago (2007). The 2006 aseismic slow slip event in Guerrero, Mexico: new results from GPS, *Geophys. Res. Lett.* **34**, L13309, doi:10.1029/2007GL029912.

Lay, T. and H. Kanamori (1981). An asperity model of great earthquake sequence in *Earthquake Production*, D. W. Simpson and P. G. Richards, Editors, American Geophysical Union, Washington, D. C., 579-592.

Lay, T., L. Astiz, H. Kanamori, and D. H. Christensen (1989). Temporal variation of large intraplate earthquakes in coupled subduction zones, *Phys. Earth Planet. Int.* **54**, 258-312.

Lermo, J., and F. J. Chavez-Garcia (1993). Site effect evaluation using spectral ratios with only one station, *Bull. Seism. Soc. Am.* **83**, 1574-1594.

Lowry, A., K. Larson, V. Kostoglodov, and R. Bilham (2001). Transient slip on the subduction interface in Guerrero, southern Mexico, *Geophys. Res. Lett.* **28**, 3753-3756.

Mai, P. M., and G. C. Beroza (2000). Source scaling properties from finite-fault-rupture models, *Bull. Seism. Soc. Am.* **90**, 604-615.

Mai, P. M., P. Spudich., and J. Boatwright (2005). Hypocenter locations in finite-source rupture models, *Bull. Seism. Soc. Am.* **95**, 965-980.

Mueller, C. (1985). Source pulse enhancement by deconvolution of an empirical Green's function, *Geophys. Res. Lett.*, **12**, 33-36.

Motazedian, D., and G. M. Atkinson (2005). Stochastic finite-fault modeling based on a dynamic corner frequency, *Bull. Seism. Soc. Am.* **95**, 995-1010.

Nakamura, Y. (1989). A method for dynamic characteristics estimation of subsurface using microtremor on the ground surface, *Q. Rep. RTRI* **30**, 25-33.

Pacheco, F. J., and Singh, S. K. (2010). Seismicity and state of stress in Guerrero segment of the Mexican subduction zone, *J. geophys. Res.*, **115**, B1303, doi:10.1029/2009JB006453.

Pardo, M., and G. Suarez (1993). Steep subduction geometry of the Rivera plate beneath the Jalisco block in western Mexico, *Geophys. Res. Lett.*, **20**, 21, 2391-2394.

Pardo, M., and G. Suarez (1995). Shape of the subducted Rivera and Cocos plates in southern Mexico: Seismic and tectonic implications, *J. Geophys. Res.*, **100**, 12,357-12,373.

Pérez-Campos, X., and G. C. Beroza (2001). An apparent mechanism dependence of radiated seismic energy, **106**, 11,127-11,136.

Rebollar, C. J., V. H. Espindola, A. Uribe, A. Mendoza, and A. Perez-Vertti (1998). Distribution of stresses and geometry of the Wadati-Benioff subduction zone at Chiapas, Mexico, *Geofis. Int.* **38**, 95-106.

Romanowicz, B. (1992). Strike-slip earthquakes on quasi-vertical transcurrent faults: inferences for general scaling relations, *Geophys. Res. Lett.*, **19**, 5, 481-484.

Schnabel, P. B., and H. B. Seed (1973). Acceleration in rock for earthquakes in the western United States, *Bull. Seism. Soc. Am.* **63**, 501-516.

Scholz, C. H. (1982a). Scaling laws for large earthquakes: consequences for physical models, *Bull. Seism. Soc. Am.* **72**, 1-14.

Singh, S. K., and M. Mortera (1991). Source time functions of the large Mexican subduction earthquakes, morphology of the Benioff zone, age of the plate, and their tectonic implications, *J. Geophys. Res.*, **96**, 21, 487-21,502.

Singh, S. K., M. Ordaz, L. Alcántara, N. Shapiro, V. Kostoglodov, J. F. Pacheco, S. Alcocer, C. Gutiérrez, R. Quaas, T. Mikumo, and E. Ovando (2000). The Oaxaca earthquake of 30 September 1999 ( $M_w = 7.5$ ): a normal-faulting event in the subducted Cocos plate, *Seism. Res. Lett.* **71**, 67-78.

Somerville, P. G., K. Irikura, R. Graves, S. Sawada, D. Wald, N. Abrahamson, Y. Iwasaki, T. Kagawa, N. Smith, and A. Kowada (1999). Characterizing crustal earthquakes slip models for the prediction of strong ground motion, *Seism. Res. Lett.*, **70**, 59-80.

Špičák, A., V. Hanuš, J. Vaněk, and M. Běhouňková (2007). Internal tectonic structure of the Central American Wadati-Benioff zone based on analysis of aftershock sequences, *J. Geophys. Res.* **112**, B09304, doi:10.1029/2006JB004318.

Strasser, F. O., M. C. Arango, and J. J. Bommer (2010). Scaling of the source dimensions of interface and intraslab subduction-zone earthquakes with moment magnitude, *Seism. Res. Lett.* **81**, 941-950.

Suárez, G., and Albin, P. (2009). Evidence for great tsunamigenic earthquakes ( $M 8.6$ ) along the Mexican subduction zone, *Bull. Seism. Soc. Am.* **99**, 892-896.

Venkataraman, A., and H. Kanamori (2004). Observational constraints on the fracture energy of subduction zone earthquakes, *J. Geophys. Res.* **109**, B05302, doi:10.1029/2003JB002549.

Vergnolle, M., A. Walpersdorf, V. Kostoglodov, P. Tregoning, J. A. Santiago, N. Cotte, and S. I. Franco (2010). Slow slip events in Mexico revised from the processing of 11 year GPS observations, *J. Geophys. Res.* **115**, B08403, doi:10.1029/2009JB006852.